4-2-2018

Thermogenic Gas Hydrate Formation In Gulf of Mexico Offshore Environment- Results from Numerical Simulation

Sulav Dhakal
Louisiana State University and Agricultural and Mechanical College, sdhaka5@lsu.edu

THERMOGENIC GAS HYDRATE FORMATION IN GULF OF MEXICO OFFSHORE ENVIRONMENT- RESULTS FROM NUMERICAL SIMULATIONS

A Thesis

Submitted to the Graduate Faculty of the
Louisiana State University and
Agricultural and Mechanical College
in partial fulfillment of the
requirements for the degree of
Master of Science

in

Craft and Hawkins Department of Petroleum Engineering

by
Sulav Dhakal
B.E., Tribhuvan University, 2013
May 2018

Acknowledgments

I would like to express my sincere gratitude to my major advisor and committee chair Dr. Ipsita Gupta, who has guided, motivated and supported me ever since I came to the university. It is hard to come from a different part of the world and adjust to life in a completely new setting, added to that the rigors of graduate school, she made it seem easy and helped me slowly ease into such a challenging research problem. I would also like to thank my committee members Dr. Karsten Thompson and Dr. Wesley Williams for their valuable insights and support during my thesis preparation and presentations. Additionally, I would like to thank Dr. Seung Kam for his technical inputs during my proposal presentation.

I am also thankful to my lab mates, German, Florencia, Makua and Hope who have endured my ramblings on gas hydrates even when they were busy doing their own research. I am grateful that I have such wonderful people working next to me who became such good friends in such a short time.

I would also like to acknowledge my friends, roommates and everyone who helped me feel at home at LSU. I am especially thankful to Dr. Puspa Adhikari and Samikshya Aryal for their continuous warmth, love and support. I am thankful for my girlfriend, Sujata Subedi, who left an already familiar environment to come and support me in this journey.

I would like to thank my parents whose selflessness and unconditional love continue to amaze me and motivate me to make them proud. This study, like everything else I do in my life, is dedicated to them. Lastly, I would like to thank everyone involved, directly or indirectly, in helping me complete this work.

Table of Contents

List of Tables

List of Figures

Abstract

Development of civilization and the resulting quest for energy have led us to previously uncharted territory in exploration and production of fuel. As the demand continues to grow and conventional oil reserves become depleted, we are looking into unconventional resources such as gas hydrates. However, due to the volatile nature of the energy market and production technology yet to perfected, we are not able to fully utilize the potential of gas hydrates yet.

Reservoir characterization of hydrates have so far been limited to seismic mapping, well log interpretation and laboratory scale studies. This research uses numerical simulation to understand the geological and thermodynamic setting in which methane hydrates form in the subsurface and the reservoir quality changes that occur during and after the formation of hydrates. A reservoir model with sand and shale layers with a fault running through them is generated and flow of thermogenic methane gas as seen in the Gulf of Mexico subsurface is simulated using TOUGH+HYDRATE, a numerical code developed at the Lawrence Berkeley National Laboratory. The code uses an integrated finite difference method for space and time discretization to simulate multiphase flow in a geological system. The model was created using a specific MATLAB code for this research. Sensitivities on boundary conditions, fault angles, flow rate and reservoir properties are performed to study the formation process of methane hydrates.

The simulation results show that the hydrate formation depends on the reservoir rock and flow parameters. The geobody distribution of hydrate was highly affected by permeability, stratigraphy, fault angles and the boundary conditions, whereas, the saturation was impacted by pore-water salinity and flow rate of the gas into the reservoir. Numerical simulation of hydrate formation and the study of the reservoir properties are an important aspect of reservoir characterization for hydrates, which can be used for production planning of methane gas from these reserves. A more robust numerical code must be developed for a reservoir scale modeling of hydrate formation to simulate detailed complexities.

Chapter 1
Background

Gas hydrates are solid compounds of gas molecules trapped in crystalline cells of water molecules. They form solid particles that resemble the structure of ice. In their natural state, they occur in polar ice caps, oceanic beds, and subsurface formations. Gases like ethane, carbon dioxide and propane can form hydrates under suitable conditions, however, in nature, methane hydrates or clathrates are the most predominantly found forms of hydrates. The first accepted discovery of hydrates is the discovery of chlorine hydrates by Sir Humphrey Davy in 1810 [53], however it is also claimed that Priestley in 1778 discovered sulphur-dioxide hydrates at atmospheric pressure and low room temperature [35]. Since then, numerous different gas hydrates have been discovered until Villard in 1888 first discovered the existence of methane, ethane and propane hydrates [53]. In the mid-1930s, it was discovered that hydrocarbon hydrates can form in natural gas pipelines to clog the gas transmission [24]. This marked the beginning of significant research on hydrates. The presence of natural gas hydrates on earth was first postulated by Russian scientists in 1960s, in which they theorized that there are hydrates in the Siberian permafrost [34]. Subsequent discovery of hydrate cores and production of gas from hydrates at the Messoyakha field in Siberia in 1970s accelerated the research efforts on gas hydrates [35]. Since then, hydrates have been touted as the next big energy resource and numerous research efforts and pilot testing have been done. In 1980, the United States Geologic Survey published the world-wide map of hydrates deposits, shown in Figure 1.1 [31]. It is estimated that there is over 15 x 10^{12} TOE of hydrated gas present on the Earth [35].

Gas hydrates are formed when gas molecules like methane or ethane (known as guest molecules) come in contact with water at temperature lower than ambient temperature and high pressure [52]. Typically, a single guest molecule is encased in water molecules forming the non-stoichiometric hydrates [52]. The repulsive force of the guest molecule depending upon the type of the molecule, determines the structure of the hydrates formed

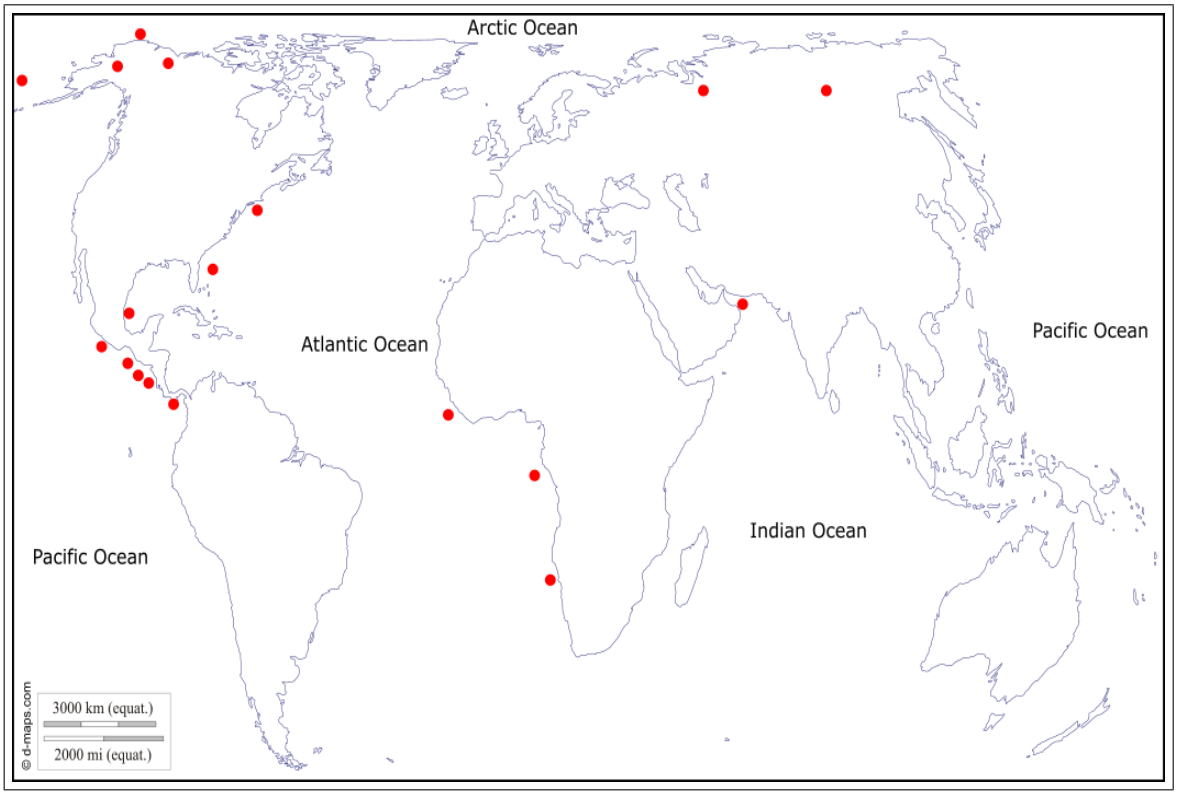

Figure 1.1: Kvenvolden and McMenamin, 1980 provided one of the early maps with gas hydrates occurrence around the world. The red dots on land surface represented suspected or confirmed gas hydrates and the dots on ocean represented areas with seismic or drilling evidence of gas hydrates presence [31].

of which three types have been observed and studied [51]. Additionally, three different kinds of morphology of hydrate crystals are found in the nature: massive, whiskery and gel-like [35].The thermodynamic conditions for the occurrence of gas hydrates has been a topic of curiosity since its discovery and a number of studies have been made and published. Several mathematical and computational methods have been developed for the prediction of such conditions [18,26,40,41,44,56]. Different models for prediction of hydrate dissociation have also been developed in conjunction, which also produce similar phase equilibrium diagrams [9,28,49].

The production of methane gas from the hydrates has been previously tested and in 2002, a joint research project between Japan, USA, Canada, Germany and India tested the production of methane gas from the Mallik site in the Mckenzie delta in Northern

Canada [55]. There have also been numerous efforts to study the presence of gas hydrates in the Gulf of Mexico [5, 10, 12, 22, 45], which is an important petroleum exploration and production region. The presence of economically feasible amounts of gas hydrates in an already developed area indicates that gas hydrate can become the energy source to drive the future.

1.1 Occurence of Gas Hydrates

Gas hydrates, especially methane hydrate, occur abundantly in natural form around the world. The amount of gas content in hydrates is determined by the structure of the hydrate. In a fully saturated methane hydrate of structure I, shown in Figure 1.2 , there are 5.75 molecules of water for each molecule of methane, and when hydrate expansion factor is considered, there can be up to 164 m^3 of methane gas at standard conditions in each $1m^3$ of hydrate [30].

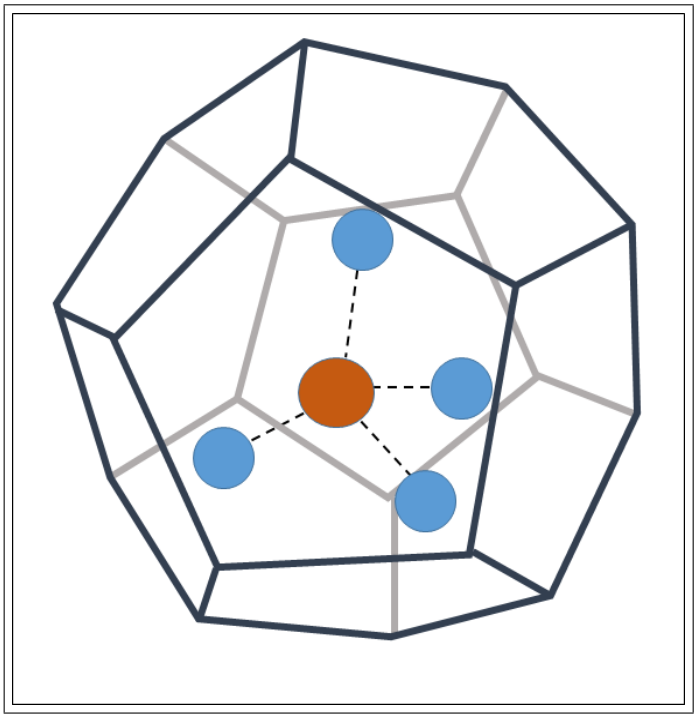

Figure 1.2: Structure I methane hydrate [52].

It is estimated that around $1.8x10^3$ Gt of carbon gas is present in gas hydrates which

corresponds to around $3x10^{15}$ m^3 of methane gas [3]. However, accurate estimation of gas hydrate resources is an extremely difficult process and significant differences may occur in different estimates using different methods [3]. In separate studies, it is estimated that $7x10^2$ to $1.27x10^4$ Gt of carbon is stored in marine gas hydrates alone while $3.75x10^2$ Gt carbon is stored in East Siberian Arctic Shelf [16, 50]. Bottom Simulating Reflector (BSR) which are the rough estimation of contrasting hydrate layer and gas saturated underlying layer indicate the presence of hydrates in subsurface seismic images [**?**]. These BSRs are used as indicators of hydrates presence in the subsurface oceanic sediments.

The amount of gas hydrates present in the earth is also subject to change due to climatic change and geologic change [15]. Gas hydrates are known to be naturally found at depths of sea floor to more than 3000 m below sea-level [53]. There is also a significant presence of gas hydrate in and below permafrost in the northern parts of the world; at concentrations from 1-2% as small and dispersed crystals to more than 90% of pore space as massive sediment displacing forms [10].

Gas hydrate as a resource is considered to be the biggest fossil fuel resource in the world; however, the term resource can be defined by either including every molecule of methane gas or by those that we can exploit by using current technology [3]. Broadly, the gas hydrate resources are divided into total gas in place (GIP), technically recoverable resources (TRR) and economically recoverable resources (ERR) [3]. Due to the shear amount of gas that is present worldwide in the form of hydrates, even a tiny fraction of producible gas can be considered as a significant resource. Field tests and research programs have shown that most of the technically recoverable hydrate resources are in coarse sandstone sediments [58]. The economically recoverable resources can vary as the global gas prices fluctuate and are intrinsically different for different field drilling techniques. In other words, recoerable resources of hydrates will continue to increase with technological advancements but at the same time will also depend on the global economic conditions. It is the economic factor

that primarily determines the production capability from the hydrates and it is suggested from simulations and pilot testing that hydrate reservoirs with underlying free gas may be economically viable [58].

1.2 Formation of Gas Hydrates

Gas hydrates are formed by phase transition requiring a supersaturated environment. The crystallization of gas hydrates occur when sufficient gas is available to dissolve in water at a high pressure and low temperature. The formation phenomenon has been modeled by using two kinetic processes (nucleation and growth) coupled with transport phenomena [18]. In most cases, the nucleation is seen at the gas-water contact as the supersaturation is higher at the interface but in some conditions, uniform supersaturation may occur before the nucleation, in which case, the nucleation is seen uniformly throughout the water [18]. Hydrate crystals can sometimes be spread in the pore spaces of the rock without disturbing the rock matrix while in some cases, the rock matrix may be affected [35].

The pressure-temperature diagram of the water-methane system (Figure 1.3) shows that hydrates are stable at a wide range of pressure and temperature; however, the right combination of pressure and temperature along with sufficient amount of free gas and water must be available in order to form hydrates [35]. The hydrate formation process is exothermic, due to which the dissociation of hydrates require a certain amount of heat provided to the system. In nature, the formation and location of gas hydrates depends on many geological and thermodynamic factors, such as the generation and migration of hydrocarbons, composition and chemical and thermodynamic properties of the gas, the structure and the lithology of the porous rock, salinity of the reservoir water, geothermal gradient and the degree of gas saturation [35]. The hydrate nucleation time is not deterministic and several different correlations are proposed depending upon the experimental apparatus used and hydrate formation condition [53]. This study uses the relationship developed by Kamath, 1984, based on experimental studies of methane hydrates and Moridis, 2002, based on re-

search data reported by Sloan, 1998. The ranges for the two relationships are shown in the Figure 1.4.

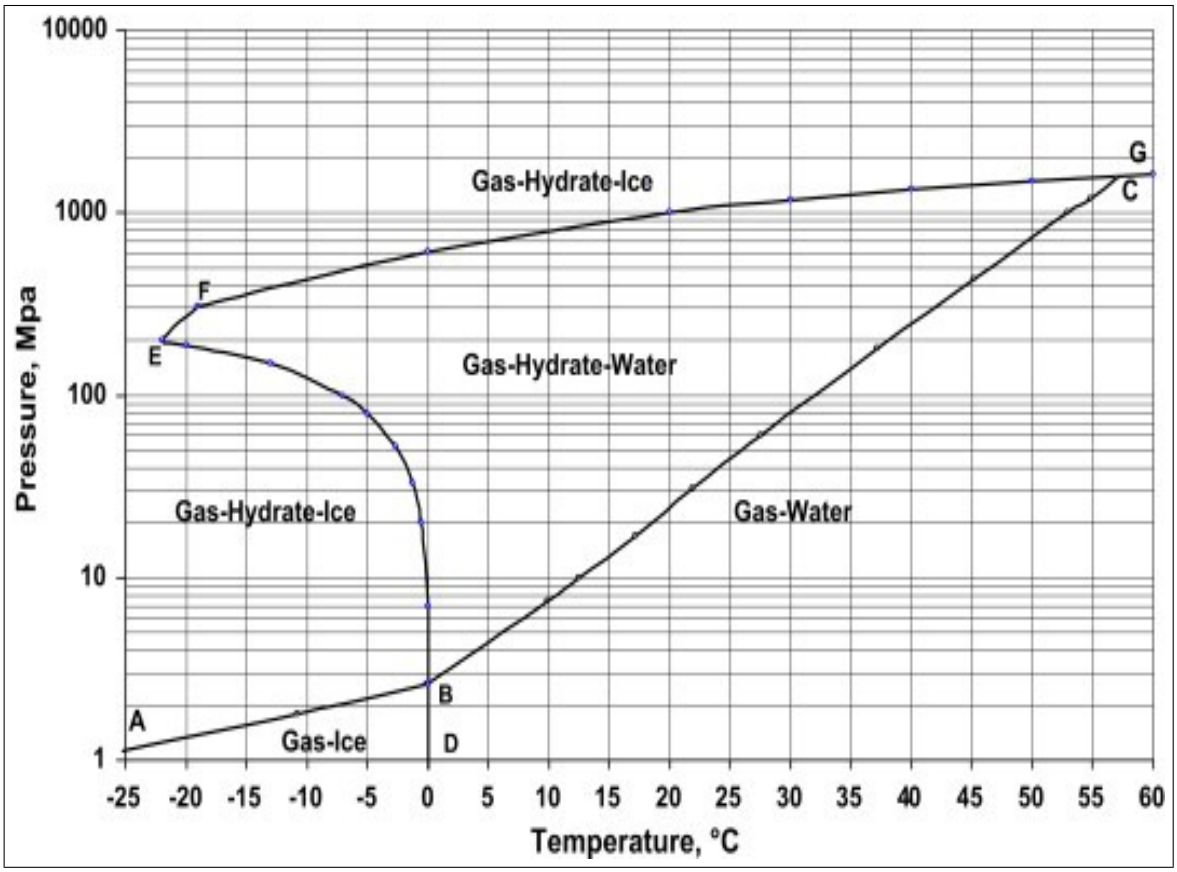

Figure 1.3: Pressure-Temperature diagram for water-methane system for hydrate formation [35].

The generation of methane gas from either biogenic or thermogenic sources, is followed by the migration of gas to hydrate stability region from the higher temperature zones [53]. The gas migration occurs through channels and faults and massive hydrate deposits are formed in areas such as the Gulf of Mexico [60], the Caspian sea [21] and Barkley Canyon, Pacific ocean [43]. It is hypothesized that the flow of hydrocarbon rich fluid up the fault due to high pressure and temperature at the subsurface into hydrate stability zone near the sea bed causes the formation and concentration of gas hydrates [43]. Hydrate cores recovered from six out of the eight known hydrate deposit sites in the Gulf of Mexico indicate that the hydrates are concentrated near or over deep faults [6]. Thermogenic gas hydrates, which

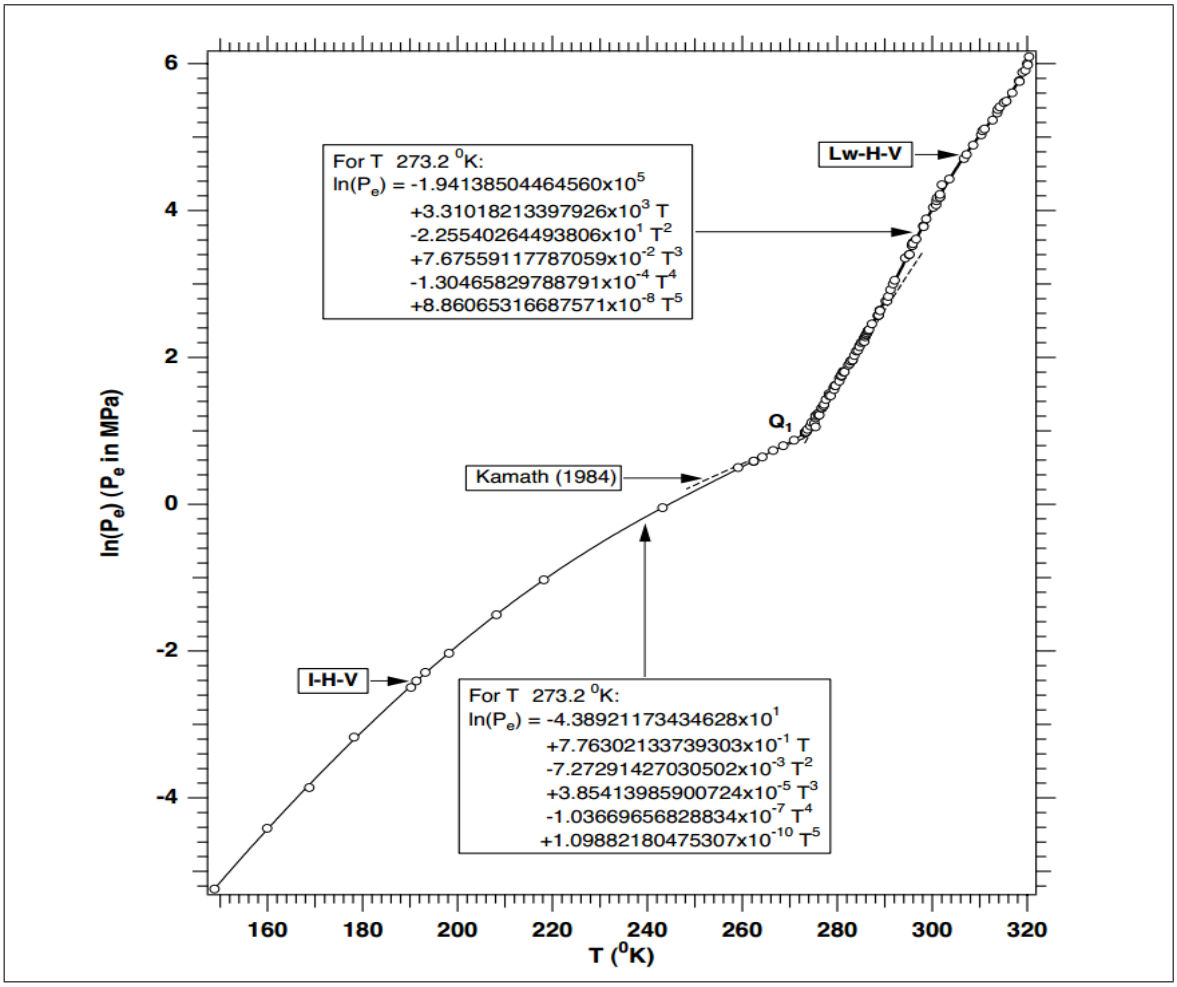

Figure 1.4: Phase relationship of hydration equilibrium pressure and temperature without inhibitor [39].

are associated with movements up faults are generally more localized than the biogenic hydrates and extensive studies have not been done on these kinds of hydrates [53].

Modeling the formation of methane hydrates is an ever evolving field with models being developed using experimental data and field observations alike. A mechanistic model based on an experimental setup of a stirred tank reactor with pressure and temperature control and describes the initial growth period of hydrates was used to describe the nucleation of hydrates [18]. An analytical model for methane hydrate formation and distribution in marine sediments was developed for two components (methane gas and water), three phase (gas hydrates, free gas and water) system by coupling conservation equations of

mass, momentum and energy [62]. Expressions describing the distribution of gas hydrate in homogeneous marine sediments were developed correlating it with observables like water depth, thickness of the hydrate stability zone, heat flux, Bottom-Simulating Reflector (BSR) depth and gas flux. While the methane hydrate stability zone is primarily dependent on the pressure and temperature of the formation, the methane hydrate zone where actual methane hydrate can be found is dependent on the availability of excess methane gas than the soluble amount [62]. Comprehensive pore scale study of hydrate formation, the structure and morphology of the pores were included to develop a meshless model for the formation of methane hydrates in marine sediments [64] . A kinetic model for methane hydrate formation due to migration of free gas was developed for Hydrate Ridge, Cascadia Margin, Oregon [8]. Free gas and water were assumed to flow up through a fault to hydrate stability zone which already contained and produced biogenic methane gas [8]. The methane hydrate stability curve in Figure 1.5 indicates that the phase boundary between gas hydrate and methane gas depends on the pressure and temperature condition [46]. Presence of inhibitors, such as salt in the water, also affects the hydrates phase equilibrium which is why marine phase diagrams and land phase diagrams are different [46].

Subsurface pressure and temperature of marine sediments is such that they increase as the depth increases. However, the hydrate phase diagram suggests that gas hydrate stability is reached at a low temperature and high pressure. Therefore, the gas hydrate stability zone is a small layer of rock where the geothermal gradient is such that hydrate stability is reached at that pressure. Marine gas hydrates thus formed have been known to have biogenic or thermogenic methane gas as their source gas. The biogenic methane gas can be formed within the gas hydrate stability zone in small areas of the porous media while thermogenic methane gas migrate upwards through faults and fractures from deeper sources.

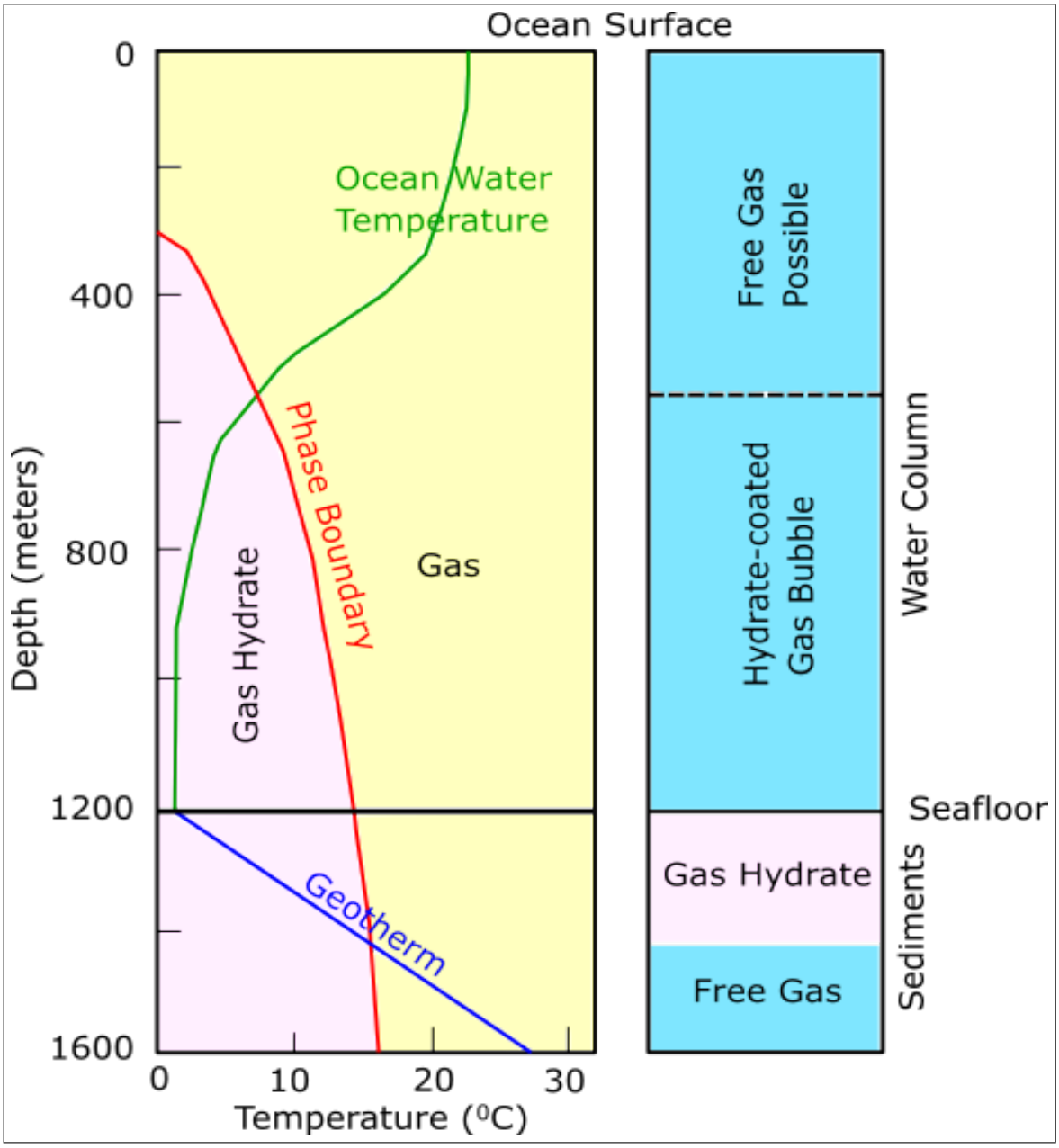

Figure 1.5: Methane hydrate stability curve for marine environments [46]

The flow of thermogenic methane gas into the gas hydrate stability zone is one of the important reasons for formation of methane hydrates in marine sediments. The primary focus of this study is to simulate thermogenic methane hydrate formation in the subsurface. Due to the deposition of gas hydrates in the pore spaces of a hydrate-bearing rock, the permeability is highly reduced and these hydrate deposits can be identified by very high resistivity and sonic velocity [35]. This study will attempt to further the understanding

of methane hydrate formation in geologic formations so as to characterize the development and/or modification of reservoir quality such that development strategies may be determined.

1.3 Gas Hydrate Reservoir Characterization

Reservoir characterization is an important step in studying the potential of any subsurface energy resource. It is a multidimensional study of a reservoir that may include tools and techniques such as well logging, core sampling, seismic imaging, well testing, production analysis, and reservoir simulation separately or in combination to facilitate an overall understanding of the reservoir and in production planning and optimization.

Hydrates reservoir characterization is a challenging task as it is a solid phase that is highly unstable when its natural temperature and pressure condition are altered. Therefore, studies such as core sampling and well logging are not very effective in estimating a hydrate reservoir's exact size and nature [63]. Reservoir characterization techniques that have been used include: seismic imaging in the Gulf of Mexico [23], well testing and production data in the Alaska and Mallik hydrate reserves [29], and core sampling and well logging data in the Gulf of Mexico [4]. Apart from these studies, material balance modeling of the Barrow gas field in Alaska was used to characterize methane hydrates and it was attempted to use CMG-STARS to model production from hydrates (not formation) [59]. Seismic imaging in the Ulleung Basin in the East Sea was used to characterize methane hydrates [27]. Gas hydrates at the Terrabone basin in the Gulf of Mexico were studied to extend the work from Joint Industry Project Leg II Logging While Drilling (LWD) project [20].

Gas hydrate reservoir characterization in marine environments is especially important as the Bureau of Ocean Management (BOEM) estimates that 607 trillion cubic meters of gas hydrates occur in the Gulf of Mexico region [4]. This could potentially be a significant future energy resource.

1.4 Gulf of Mexico Gas Hydrate Occurrence

The Gulf of Mexico is a well studied area with a long history of oil and gas exploration and production. There were early indication and detection of gas hydrate bearing sediments in the Gulf of Mexico continental slope through academic researches [7, 33, 48]. As deepwater drilling in the area increased, the hazards related to drilling through hydrates were realized and a need to understand the magnitude, type and structure of subsurface hydrates arose [25]. As a result, the Gulf of Mexico Gas Hydrates Joint Industry Project (JIP) was formed in 2001 with the management of Chevron and the involvement of ConocoPhillips, Schlumberger, Total, Halliburton, Reliance Industries, the Japan Oil Gas and Minerals Economic Corporation, and the U.S. Minerals Management Service [45]. The JIP mainly focused on laboratory studies of hydrates, numerical simulations of borehole stability, development of core analysis tools and processing of existing seismic data before the leg I drilling expedition at Atwater Valley and Keathley Canyon that studied the gas hydrate occurrence and wellbore stability while drilling through it [45].

For further study of gas hydrates in the Gulf of Mexico, the JIP drilling expedition leg II began drilling in 2009 at three different locations in the Gulf of Mexico. The expedition employed drilling while logging tools at Alaminos Canyon, Green Canyon and Walker ridge found evidence of gas hydrates as thick as 30 m in the form of hydrate rich sandstone [11, 12, 22].

The two drilling expeditions were an important step in the study of gas hydrates in the Gulf of Mexico as that paved the way for study of gas hydrates in the Gulf of Mexico as the International Ocean Drilling Program (IODP) had previously notably omitted the Gulf of Mexico region from its expeditions [45].

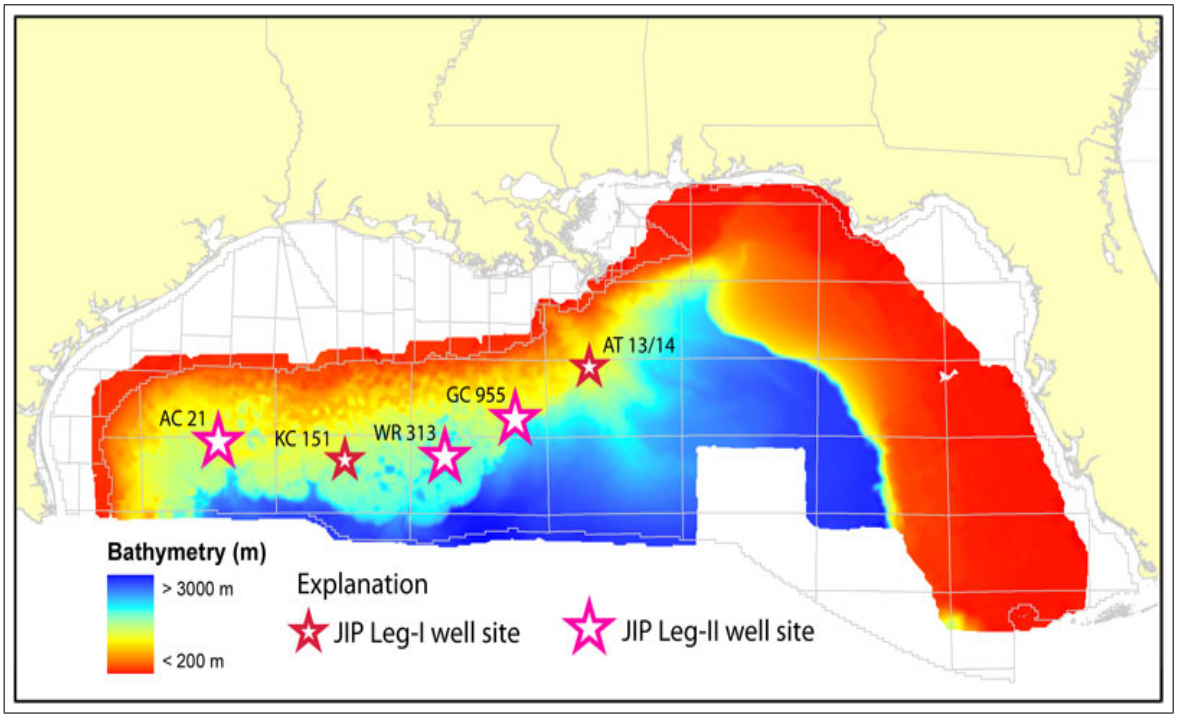

Figure 1.6: Joint Industry Project Drill Sites in the Gulf of Mexico (USGS)

Characterization of gas hydrates in the Gulf of Mexico was another step in the study of hydrates in the region. The methods used however have been limited to static methods of seismic imaging, core analyses and well logging. Seismic imaging of gas hydrate systems at the major locations that were drilled in the joint industry project expeditions show prolific presence of these gas hydrates [14, 23, 54]. Figure 1.7 shows images from three intersecting seismic 2D lines used to characterize hydrate bearing sediments at the Green Canyon site in the Gulf of Mexico.

The seismic images show a gas migration system and hydrate accumulations near two wells, GC955-Q and GC955-H. There are chimney features that indicate free gas movement through fault zones. There are hydrate accumulations near the GC955-H well; whereas, at the proximity of the GC955-Q well, a lack of visible flow conduits connecting the free gas zone with sand layers also coincides with lack of hydrate accumulation [23].

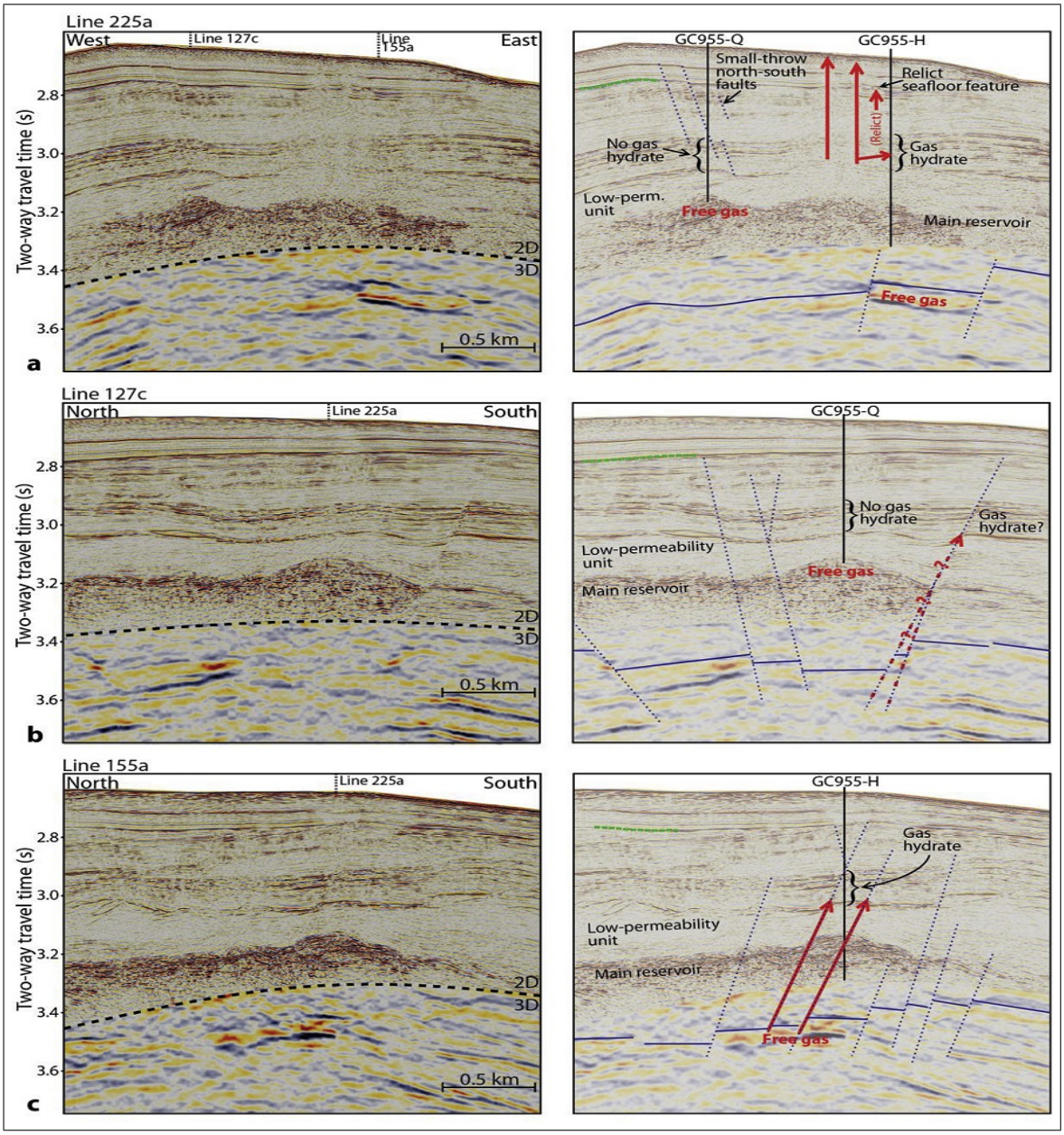

Figure 1.7: Seismic image indicating presence of gas hydrates in the Gulf of Mexico at the Green Canyon 955 site [23]

The seismic evidence of hydrate formation above the fault zones is directly tied with this study where it is attempted to simulate the formation of gas hydrates with fault zone acting as a flow conduit. The contrasting conditions caused by the presence of fault zones around the two wells give an indication of the hydrate formation phenomena in oceanic sediments.

Chapter 2
Objectives

The main hypothesis of this research is that hot fluids (methane, water and a combination) moving up faults during the latter's activation periods generate gas hydrate deposits in subsurface formations where hydrate stability pressure and temperatures regimes dominate or are attained, and the spatial and temporal distribution of these unconventional resources are a function of the fluid regime, stratigraphy, and structure of the reservoirs and their adjacent formations (geologic sequence).

To that effect, the objectives of this study are to:

1. Numerically simulate coupled fluid and heat flow and solute transport through faults to generate (form) gas hydrate deposits in the geologic subsurface.

2. Quantify the resultant reservoir quality changes (in particular properties such as porosity and permeability) as a result of the invasion of these hot gases into sedimentary formations, typical of Gulf of Mexico.

3. Understand the impact of varying fault angles (structure) on the spatial distribution of the gas hydrate formation.

4. Understand the impact of varying stratigraphy (sand/shale sequences) on the spatial distribution of gas hydrates.

5. Develop a method for numerical reservoir characterization using reservoir simulation principles - hydrates reservoirs are mainly characterized using seismic imaging, logging and core sampling. This research will generate a quantitative method of characterization for such reservoirs.

6. Understand the impact of the spatial distribution of gas hydrates on future development of these resources, i.e. future work on well placements, reservoir management, production methods and strategies.

Chapter 3
Methodology

3.1 Methane Hydrates Formation Modeling

Methane hydrate formation can be represented by the simple equation [38]:

$CH_4 + N_H\, H_2O \longrightarrow CH_4 \cdot N_H\, H_2O$

Where, N_H is the hydration number that depends on the thermodynamic state of the hydrate formation. For methane, the average hydration number in nature is about 6 [38]. The hydrate forming gases are usually not a single gas component in nature, which is why composite hydrate formation reaction must be taken into account for a more realistic approach to hydrate modeling. Gases such as carbon dioxide, ethane, hydrogen sulfide, and nitrogen form hydrates with different hydration numbers. For the sake of simplicity most models usually take only one or two gas components into consideration.

Numerical simulation of methane hydrate formation is done using TOUGH+HYDRATE v1.5. It is a numerical code developed at Lawrence Berkeley National Laboratory. The TOUGH+HYDRATE code is written using FORTRAN 95/2003. It is able to simulate non-isothermal fluid flow for studying the behavior of methane hydrates in porous and fractured media. It solves coupled mass and heat balance equations to model different scenarios of phase behavior, fluid flow and heat transfer for methane hydrates. It includes an equilibrium as well as kinetic model of hydrate formation and dissociation. In this study, the equilibrium model will be used because of its lesser computational cost and run time. The code takes into account three components, water, methane and inhibitor and four phases, gas, liquid, ice and hydrate, while heat is also considered as a pseudo-component to track heat balance in the system. Hydrate is considered a component as well as a phase in the kinetic reaction and only a phase in the equilibrium reaction [38]. The TOUGH+HYDRATE code was primarily written to model the dissociation of methane hydrate but it is also capable of modeling its formation as it takes the phase diagram as the delineating limits of

hydrate formation and dissociation. Inclusion of inhibitor and its properties in the code allows for the simulation of behaviors of inhibitors like salt and alcohol in hydrate bearing sediments. The TOUGH+ code uses the integrated finite difference method to discretize geometry data and time discretized as first order finite difference. Some assumptions are made in the simulation code to simplify the model and reduce computational costs [38]. These include:

1. The flow in the simulation domain is based on Darcy's law, which means Non-Darcy's flow is not considered.

2. Mechanical dispersion is not considered in the transport of dissolved gas and inhibitors.

3. Movement of the rock matrix material is not considered while simulation of fluid flow, and effects of pressure of flow is computed by using pore compressibility of the medium.

4. Precipitation of dissolved salt is not considered and salt is considered to be present in dissolved form

5. Due to computational constraints, the effect of dissolved inhibitors on thermo-physical properties of water are not considered.

6. The upper limit of pressure is kept at 100 MPa due to the fact that the maximum pressure at which natural hydrates are known to exist is 11 MPa [38].

7. The flow of gas component considered in this study only includes methane (CH_4) due to computational constraints in including other components found in nature such as ethane, carbon dioxide, propane, etc.

The TOUGH+HYDRATE code is a part of a larger executable suite called TOUGH+CORE that can be used to model other various types of fluid flow in geological media. The TOUGH+CORE code uses the following terms to simulate the fluid flow model.

1. Mass and energy balance equation

$\frac{d}{dt}\int\limits_{V_n} M^{\kappa} dV = \int\limits_{\Gamma_n} F^{\kappa}.n \, d\tilde{A} + \int\limits_{V_n} q^{\kappa} dV,$

where

V,V_n = Volume, Volume of subdomain n [m^3];

M^k = Mass accumulation term of component [kg m^{-3}];

A, Γ_n = Surface area, surface area of subdomain n [m^2];

F^k = Darcy flux vector of component K [kg $m^{-2}s^{-1}$];

n = Inward unit normal vector;

q^x = Source/sink term of component k [kg m^{-3} s^{-1}];

t = Time [s]

2. Mass accumulation terms

$M^{\kappa} = \sum\limits_{\beta=A,\, G,\, I,\, H} \phi \, S_{\beta} \, \rho_{\beta} X_{\beta}^{\kappa}, \qquad \kappa \equiv w, m, i$

where

ϕ = Porosity [dimensionless];

ρ_{β}= Density of phase β [kg m^{-3}];

X_{β}^{κ} = Mass fraction of component X in phase β [kg/kg];

In the equilibrium model that is used in this study, different cases of β give the following relations:

$\beta = G : X_G^i = 0$

$\beta = H : X_H^w = \frac{W^m}{W^h}$, $X_M^m = 0$, $X_H^w = 0$

$\beta = 1, X_I^m = X_I^i = 0$, $X_I^w = 1$

The terms W^m and W^k represent the molecular mass of methane gas and of methane hydrate respectively.

The void number N_v (pore space) is assumed to be equal to the number of grains and the void volume V_v is computed as

$N_v = \frac{1-\phi}{\mathrm{V_P}}$, $V_v = \frac{1-\phi}{\mathrm{N_v}}$

At any time t, a representative methane hydrate particle radius $\mathrm{r_H}$ and $\mathrm{V_H}$ are computed as

$\mathrm{V_H} = \frac{\phi \mathrm{S_H}}{\mathrm{N_V}},\ \mathrm{r_h} = \mathrm{r_V}\left(\frac{\mathrm{V_H}}{\mathrm{V_V}}\right)^{\frac{1}{3}} = \mathrm{r_V S_H^{\frac{1}{3}}}$

And the hydrate reactive area is computed as

$\mathrm{A} = \mathrm{f_A A_{TV}}\left(\frac{\mathrm{r_H}}{\mathrm{r_V}}\right)^2 = \mathrm{f_A N_V}\left(4\pi \mathrm{r_p^2}\right)\mathrm{S_H^{\frac{2}{3}}}$

Given the intrinsic permeability k of a porous medium, the Kozeny-Carman Equation gives an estimate of the effective radius $\mathrm{r_p}$ of the grains as [1]

$\mathrm{r_P} = \left[45\mathrm{k}\frac{(1-\phi)^2}{\phi^3}\right]^{\frac{1}{2}}$

3. Heat accumulation terms

The heat accumulation term is given by the following equation [38]

$\mathrm{M}^{\theta} = (1-\phi)\rho_{\mathrm{R}}\mathrm{C_R T} + \sum_{\beta=1,\ldots\mathrm{N}_\beta} \phi \mathrm{S}_\beta \rho_\beta \mathrm{U}_\beta + \mathrm{Q_{diss}},$

$Q_{\mathrm{diss}} = \Delta(\phi\rho_{\mathrm{H}})\mathrm{S_H}\Delta\mathrm{H}^0$ for equilibrium formation of methane hydrates,

Where ρ_{R} = Rock density [$\mathrm{kgm^{-3}}$];

$\mathrm{C_R}$ = Heat capacity of dry rock [$\mathrm{J\ kg^{-1}K^{-1}}$];

U_β = Specific internal energy of phase β [$\mathrm{J\ kg^{-1}}$];

$\Delta()$ = Change in the quantity in parantheses over the current time step;

4. Flux terms

The mass fluxes of water, methane and inhibitor include contributions from the aqueous and gaseous phases, i.e,

$\mathrm{F}^{\kappa} = \sum_{\kappa \equiv \mathrm{A,G}} \mathrm{F}^{\kappa}_{\beta}$, where, $\kappa \equiv \mathrm{w},\ \mathrm{m}, \mathrm{i}$

The mass flux of hydrate ($\kappa \equiv h$) is $N_{m\beta}$ which is the number of mobile phases.

$\mathrm{F}^{\mathrm{h}} = 0$

For the aqueous phase, $\mathrm{F}^{\mathrm{w}}_{\mathrm{A}} = \mathrm{X}^{\mathrm{w}}_{\mathrm{A}}\mathrm{F}_{\mathrm{A}}$, and the phase flux F_{A} is described by Darcy's law as,

$\mathrm{F}_{\mathrm{A}} = -\mathrm{k}\frac{\mathrm{k_r A}\rho_{\mathrm{A}}}{\mu_{\mathrm{A}}}(\nabla \mathrm{P}_{\mathrm{A}} - \rho_{\mathrm{A}}\mathrm{g})$,

where

k = Rock intrinsic permeability [m^2];

$\mathrm{k_{rA}}$ = Relative permeability of the aqueous phase[dimensionless];

μ_A = Viscosity of the aqueous phase [Pa s];

$\mathrm{P_A}$ = Pressure of the aqueous phase [Pa];

g = Acceleration due to gravity [ms^{-2}];

The methane solubility in the aqueous phase is related to $\mathrm{P}^{\mathrm{m}}_{\mathrm{G}}$ through Henry's law,

$\mathrm{P}^{\mathrm{m}}_{\mathrm{G}} = \mathrm{H}^{\mathrm{m}}\mathrm{X}^{\mathrm{m}}_{\mathrm{A}}$

where

$\mathrm{H}^{\mathrm{m}} = \mathrm{H}^{\mathrm{m}}(\mathrm{T})$ = Temperature-dependent Henry's coefficient

The mass flux of the gaseous phase ($\beta = G$) incorporates advection and diffusion contributions, and is given by

$\mathrm{F}^{\kappa}_{\mathrm{G}} = \ -\mathrm{k}_0\frac{\mathrm{k_{rG}}\rho_{\mathrm{G}}}{\mu_{\mathrm{G}}}\mathrm{X}^{\kappa}_{\mathrm{G}}\left(\nabla \mathrm{P}_{\mathrm{G}} - \rho_{\mathrm{G}}\mathrm{g}\right) + \mathrm{J}^{\kappa}_{\mathrm{G}},\ \kappa \equiv \mathrm{w}, \mathrm{m}$

where $\mathrm{k_G} = \mathrm{k}_0\left(1 + \frac{\mathrm{b}}{\mathrm{P}}\right)$;

k_0 = Absolute permeability at large gas pressures ($= \kappa$) [m^2];

b = Klinkenberg b-factor accounting for gas slippage effects [Pa];

$\mathrm{k_{rG}}$ = Relative permeability of the gaseous phase [dimensionless];

μ_{G} = Viscosity of the gaseous phase [Pa s].

$\mathrm{J}_{\mathrm{G}}^{\kappa}$ = Diffusive mass flux of component κ in the gas phase [kg/m^2/s],

Diffusion is not expected to impact the flow of gas as much as advection in the flow of methane gas through a fault zone [38] and hence is not included in this study.

The heat flux takes into account the conduction, advection and radiative heat transfer, and is given by

$$\mathrm{F}^{\theta} = -\bar{\mathrm{k}}_{\theta}\nabla\mathrm{T} + \mathrm{f}_{\sigma}\sigma_0\nabla\mathrm{T}^4 + \sum_{\beta=\mathrm{A,G}} \mathrm{h}_{\beta}\mathrm{F}_{\beta},$$

where

$\bar{\mathrm{k}}_{\theta}$ = Composite thermal conductivity of the rock-fluids ensemble [W m^{-1}K^{-1}];

h_{β} = Specific enthalpy of phase $\beta \equiv$ A. G [J kg^{-1}];

f_{σ} = Radiance emittance factor [dimensionless];

σ_0 = Stefan-Boltzmann constant [5.668710^{-8} J m^{-2} K^{-4}].

The specific enthalpy of the gas phase is computed as:

$$\mathrm{H_G} = \sum_{\kappa\equiv\mathrm{w,m}} \mathrm{X}_{\mathrm{G}}^{\kappa}\, \mathrm{h}_{\mathrm{G}}^{\kappa} + \mathrm{H_{dep}}$$

where

$\mathrm{h}_{\mathrm{G}}^{\kappa}$ = Specific enthalpy of component κ in the gaseous phase;

$\mathrm{H_{dep}}$ = Specific enthalpy departure of the gas mixture [J kg^{-1}].

The specific enthalpy of the aqueous phase is estimated from [38]

$$\mathrm{H_A} = \mathrm{X_A^w h_A^w} + \mathrm{X_A^m}\left(\mathrm{h_A^m} + \mathrm{H_{sol}^m}\right) + \mathrm{X_A^i}\left(\mathrm{h_A^i} + \mathrm{H_{sol}^i}\right),$$

where

$\mathrm{h_A^w}$, $\mathrm{h_A^m}$ and $\mathrm{h_A^i}$ are the specific enthalpies of H_2O, CH_4, and the inhibitor at the conditions prevailing in the aqueous phase, respectively, [J kg^{-1}].

$\mathrm{H_{sol}^m}$ and $\mathrm{H_{sol}^i}$ are the specific enthalpies of dissolution [J kg-1] of CH4 and of the inhibitor in the aqueous phase, respectively [J kg^{-1}].

5. Source and sink terms

   The source and sink terms are defined by the equation [38],

   $$\hat{q}^{\kappa} = \sum_{\beta=1,\ldots,\, N_{m\beta}} X_{\beta}^{\kappa}\, q_{\beta},\ \kappa \equiv w, m$$

   Where

   q_{β} = Mass production rate of the mobile phase β [kg/m^{-3}]

   The production rate Q_m [kg m^{-3} s^{-1}] of CH_4 is computed by,

   $Q^m = \frac{W^m}{W^c} Q_H$,

   The hydrate-related release of water Qw is determined from the stoichiometry as presented by $Q^w = -\frac{N_m W^w}{W_C} Q_H$

   In equilibrium conditions, which is the case used in this study, the heat removal rate or addition rate include (a) the heat associated with fluid removal or addition, and (b) direct heat inputs or withdrawals, and is described by

   $$\hat{q}^{\theta} = q_d + \sum_{w \equiv A,\, G} h_{\beta} q_{\beta}$$

3.2 Development of Initial Model

The base case geological model is created using a MATLAB code (see Appendix) specifically developed for this study. TOUGH+ uses a text file to define geometry of reservoir, which includes elements and connections. Since, it uses an Integrated Finite Difference method for discretization, the element co-ordinate is defined as the center of the element. TOUGH+ includes its own model creation tool, Meshmaker, but it is limited in choice regarding the geometry of zones. Each zone created in Meshmaker can only be either cartesian cuboid or radial in geometry, albeit they can be rotated on the horizontal axis. The model developed for this study does not fit either category due to the presence of an inclined fault zone running through horizontal sandstone and shale layers. Therefore, a MATLAB code was developed to incorporate an inclined fault zone.

Due to the simplistic nature of the TOUGH+ mesh format, a simple text editing code is developed for this purpose using MATLAB. By defining a matrix for the elements, all other elemental properties such as zone, element volume, area and sizes are stored as cell values in the matrix. Another matrix is defined for the connections and vertical and horizontal connections with elements are defined with connection properties. Since the elements need to be given an initial condition, it is also defined in another matrix and all the information is written in respective text files for elements, connections, and initial conditions. Figure 3.1 shows the base case model developed from the MATLAB code.

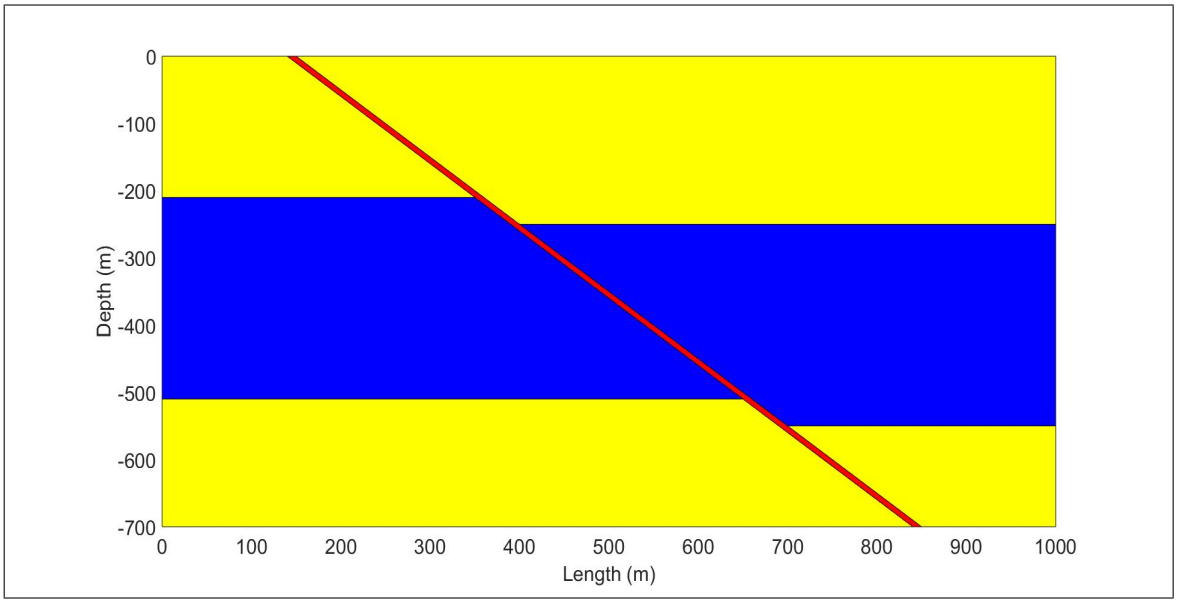

Figure 3.1: Basecase model defined from the MATLAB code. Blue: Sandstone, Red: Fault zone, Yellow: Shale.

3.3 Basecase Model

The model developed for this study is a two dimensional cross-section of a sandstone and shale sequence cross-cut with a normal fault off-setting them. The fault zone is 10 m wide. Fault angle in the base case model is 45^0. The grid size for the basecase model is 5m X 5m. The horizontal layers are shale, sand and shale sequence (Figure 3.2). The total vertical depth (TVD) of the model is assumed to be at 700m below the seafloor with no flow boundaries on the top and sides. Methane gas is injected through the bottom of the

fault zone simulating the flow of thermogenic methane gas up through the fault during a fault activation period. The top shale layer is 250m thick , the sand layer is 300m with an upthrow of 40m along the fault. The sand layer thickness was kept at a much larger thickness than the average gas hydrate stability zone thickness at such depth to facilitate the flow of gas and formation of hydrates in a suitable hydrate equilibrium pressure and temperature zone. The average porosity of the shale layers is 15%, that of sand layer is 35% and the fault zone has 50% porosity in the base case model [36]. Initially, the model is fully saturated with water with no free gas or dissolved gas present. The top of the model is at a hydrostatic pressure of 20.89809 MPa and the temperature of 10 ^{0}C with pressure gradient of 0.01 MPa/m and geothermal gradient of 0.032 ^{0}C/m [19]. Methane gas flow through the fault is simulated using injection cells at the bottom of the fault zone at a constant rate of 3E-3 kg/s at a specific enthalpy of 3.463e+05 J/kg [2,32]. The gas flow through the fault is not constant in nature [23] but for this study it was assumed to be constant for simplicity and lack of exact values of rate and the frequency of flow of thermogenic methane. In this study, geomechanical coupling is not implemented and an empirical relation [47] between porosity and permeability is used. Relative permeability of gas and aqueous phases are given by Coreys curve [13] represented by the equations below.

$k_{rA} = \hat{S}^4$ And $k_{rG} = \left(1 - \hat{S}\right)^2 \left(1 - \hat{S}^2\right)$

where $\hat{S} = \frac{S_A - S_{iA}}{1 - S_{irA} - S_{irG}}$; S_{irA} and S_{irG} are the irreducible water and gas saturation used as 0.12 and 0.02 respectively. Figure 3.2 shows the schematic basecase model.

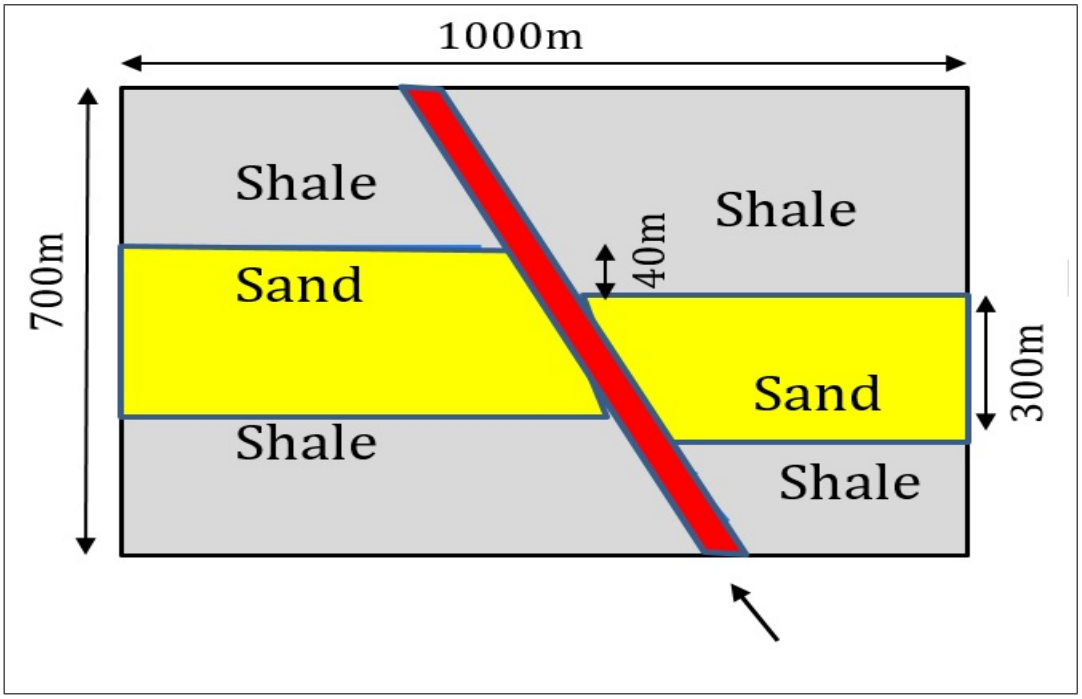

Figure 3.2: Schematic 2-D basecase simulation model (Not-to-Scale)

The capillary pressure function for two phases is given by the van Genuchten function [57]. TOUGH+HYDRATE implements an automatic time-step adjustment which is also used in this study. For simplicity of the simulation, overshoot values for equilibrium pressure, temperature and saturation of 1E-3 each was introduced. Other model parameters are listed in Table 3.1 [36].

Table 3.1: Basecase Model Parameters

SN	Property	Sandstone	Shale	Fault
1	Rock Grain Density	2650 kg/m^3	2710 kg/m^3	2650 kg/m^3
2	Porosity	0.35	0.15	0.50
3	Permeability	1.0E-12 m^2 (H) 1.0E-13 m^2 (V)	1.0E-14 m^2 (H) 1.0E-15 m^2 (V)	1.0E-11 m^2 (H) 1.0E-11 m^2 (V)
4	Pore Compressibility	3.6E-6 psi^{-1} (5.221E-10 Pa^{-1})	6.3E-6 psi^{-1} (9.137E-10 Pa^{-1})	3.6E-6 psi^{-1} (5.221E-10 Pa^{-1})

3.4 Sensitivity Analyses

To account for differences in geologic structure, stratigraphy, fault activation periods, and resultant fluid flow rates, sensitivity analyses were performed to assess the impact of these parameters on the distribution of gas hydrate formation, and the resultant diagenetic changes in porosity and permeability (reservoir quality).

3.4.1 Fault Angle

The base case model had a normal fault with a fault angle of 45^0. Assuming that the fault angle would affect the fluid flow pattern and thus the formation of gas hydrates, the fault angle was varied 40^0 to 90^0 in order to model different flow conditions with different flow paths. The nature of flow of gas with different fault angles is an important parameter to study as the gas flow velocity would be affected by the fault inclination and resultant driving mechanism of flow.

3.4.2 Stratigraphy, Permeability and Flow Rate

The formation of gas hydrate and its dependency on the stratigraphy of the sand and shale layers is also studied. By changing the position of the sand layer and its depth, different models are run to study the nature of gas hydrate formation. Permeability of the rock layers are changed by the order of 10 to study the impact of low permeability as well as high permeability of sand and shale layers on the nature of gas flow, hydrate formation rate, geobody formation and size. Flowrate of methane gas is changed from 3E-2kg/s to 3E-7 kg/s by the order of 10 in order to understand the nature of hydrate formation and the running of numerical code.

3.4.3 Boundary Conditions

Boundary condition is another parameter that greatly impacts the pressure of the system and the nature of fluid flow within the model. Therefore, the boundary condition

is changed from Neumann no-flux boundary condition to Dirichlet boundary conditions on the sides and at the top. The default boundary condition in TOUGH+HYDRATE is the no flux Neumann boundary condition, which is applied on the basecase model. To understand the effect of continuous flow through the top and the side boundaries, Dirichlet boundary conditions are also implemented on the top and sides. The Dirichlet boundary condition is mimicked in TOUGH+HYDRATE using a very large element on the top layer.

3.4.4 Inhibitor Concentration

Inhibitor concentration in the reservoir also determines the hydrate formation in the subsurface. Salt acts as an inhibitor in the hydrate nucleation reaction and since this study is aimed to study the formation of hydrates in oceanic sediments, salt concentration is a parameter that is used for sensitivity analyses. It is estimated that for a pressure range of 2.5 MPa to 10 MPa, the hydrate equilibrium temperature decreases by 1.1 ^{0}C [17]. The inhibitor concentration is changed to 35g/l which is the average salinity of Gulf of Mexico pore water [37]. Table 3.2 shows the parameters changed during the sensitivity analyses.

Table 3.2: Sensitivity Analyses Description

SN	Property	Parametric Change
1	Fault Angle	40^0 to 90^0
2	Flow Rate	2E-2 kg/s to 2E-7 kg/s
3	Permeability	Basecase Permeability X 0.1 Basecase Permeability X 10
4	Boundary Condition	Dirichlet Boundary on sides Dirichlet Boundary on top Dirichlet Boundary on top and sides
5	Stratigraphy	Sand layer 100m Sand layer 200m Sand layer 400m
6	Inhibitor concentration	0 g/l 35 g/l

All the simulations in this research are performed using a serial license of modified version of TOUGH+HYDRATE at the High Performance Computing center at Louisiana State University.

Chapter 4
Results and Discussion

4.1 Basecase Model Results

A basecase model was used as a metric for understanding the process of hydrate formation in the subsurface. The base case model is a 2-D sand-shale sequence with a 45^0 normal fault off-setting them (Figure 3.1). Methane is injected through the bottom of the fault to mimic fault activation and migration of fluids from deeper formations.

Results indicate that as methane invades the sand formation, the free gas volume increases linearly (Figure 4.1) until the first hydrate crystals start nucleating (in this macro-scale model, the first hydrates forming). With increasing hydrates in the reservoir, the free gas volume in the formation reduces, but not all of the available gas immediately turns into methane hydrates.

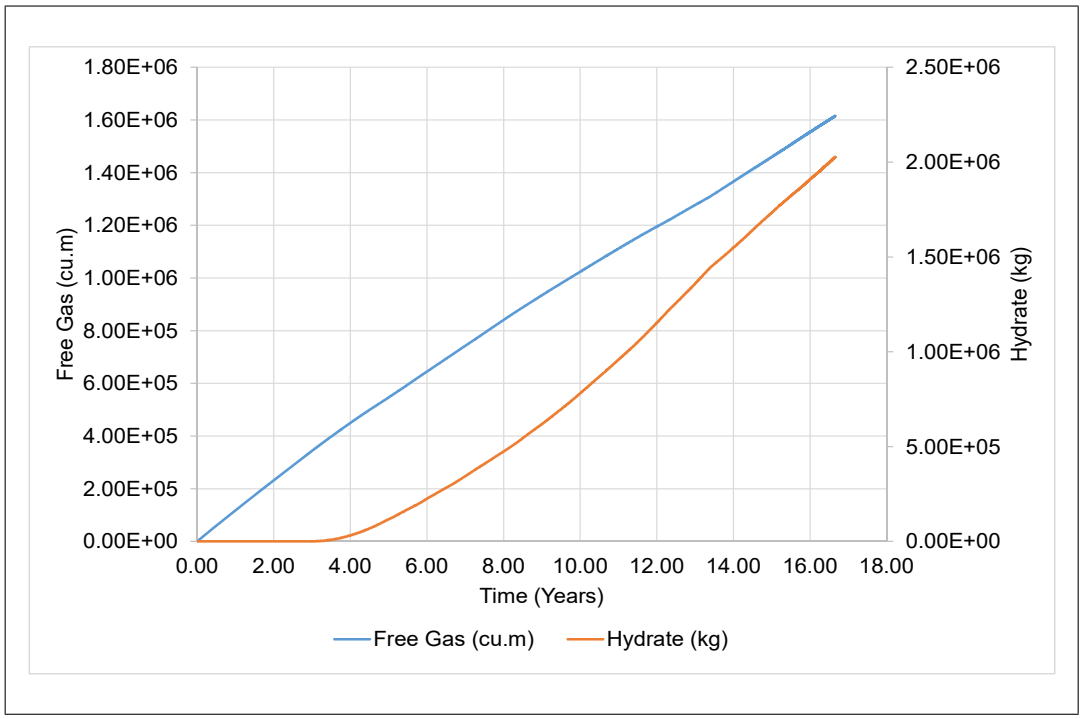

Figure 4.1: Basecase result: Free methane gas and methane hydrate in the reservoir

The basecase model is able to generate 2027797.3 kg of hydrates by 17 years at a constant injection rate of 3E-3kg/s. This is in alignment with Haines et al., 2017 who reported a volume of 4E-6 m^3 which is a three dimensional estimate from seismic data. Thus, the basecase model is replicative of Gulf of Mexico subsurface gas hydrate formations. What must be noted, however, is the fact that at this time it is difficult to predict whether the gas hydrate volumes generated in this model (basecase) could actually form within 17 years of fault activation. A computational simplification is made here with constant injection rates for a span of several years until hydrate volumes analogous to those reported in literature are formed. However, fault activation in geologic history may last several 100s of years, may be episodic, may first appear as leaks and then high rates of flow may occur [42,61] in other words there is considerable uncertainty and heterogeneity of resultant fluid flow rates that may occur as a result of instant or episodic fault activation periods which is not captured in these simulations here. This however does not deter from the fact that the basecase model was able to generate volumes of gas hydrates that are similar to volumes reported in literature.

The boundary between the sand and shale regions is where the gas hydrate stability condition is matched as temperature change shifts the base of the gas hydrate stability zone, the gas starts to nucleate into hydrates and hydrate saturation increases along the bottom of the shale layer. Figure 4.2 shows that there is some amount of hydrates forming in the sand zone but it is insignificant since the gas continues to move upwards and with it, the saturation front of hydrate also moves up and as it moves sideways in the shale layer hydrate saturation front also moves.

It is also seen that along the top of the reservoir model, which is also the bottom of the sea floor, provided that there is an impermeable boundary to stop methane flux into the ocean, hydrates start accumulating. The hydrate at the top of the fault zone is seen mostly accumulating along the boundary of the fault zone and within the adjoining sediments.

Thermogenic hydrate formation at the top of the fault zone, horizontal beds, around the flow conduits and at the sea floor have been observed in past studies which validates the result from this study [23, 33, 48]. The saturation seen at the hydrate bearing horizontal sand and shale layers is also within the range of observed hydrate saturations in the Gulf of Mexico [23].

Vertical sections of the reservoir at 150m, 500m, 700m and 900m are plotted with hydrate saturation at different depths (Figure 4.3) and it is observed that the hydrate saturation at the top of the model near the sea floor is the highest which can be seen from Section A-A. The hydrate saturation at the shale layer is almost uniformly distributed at the three Sections B-B, C-C and D-D. This effect can be attributed to the low vertical permeability of the shale layer and a uniform distribution of gas before nucleation into hydrates.

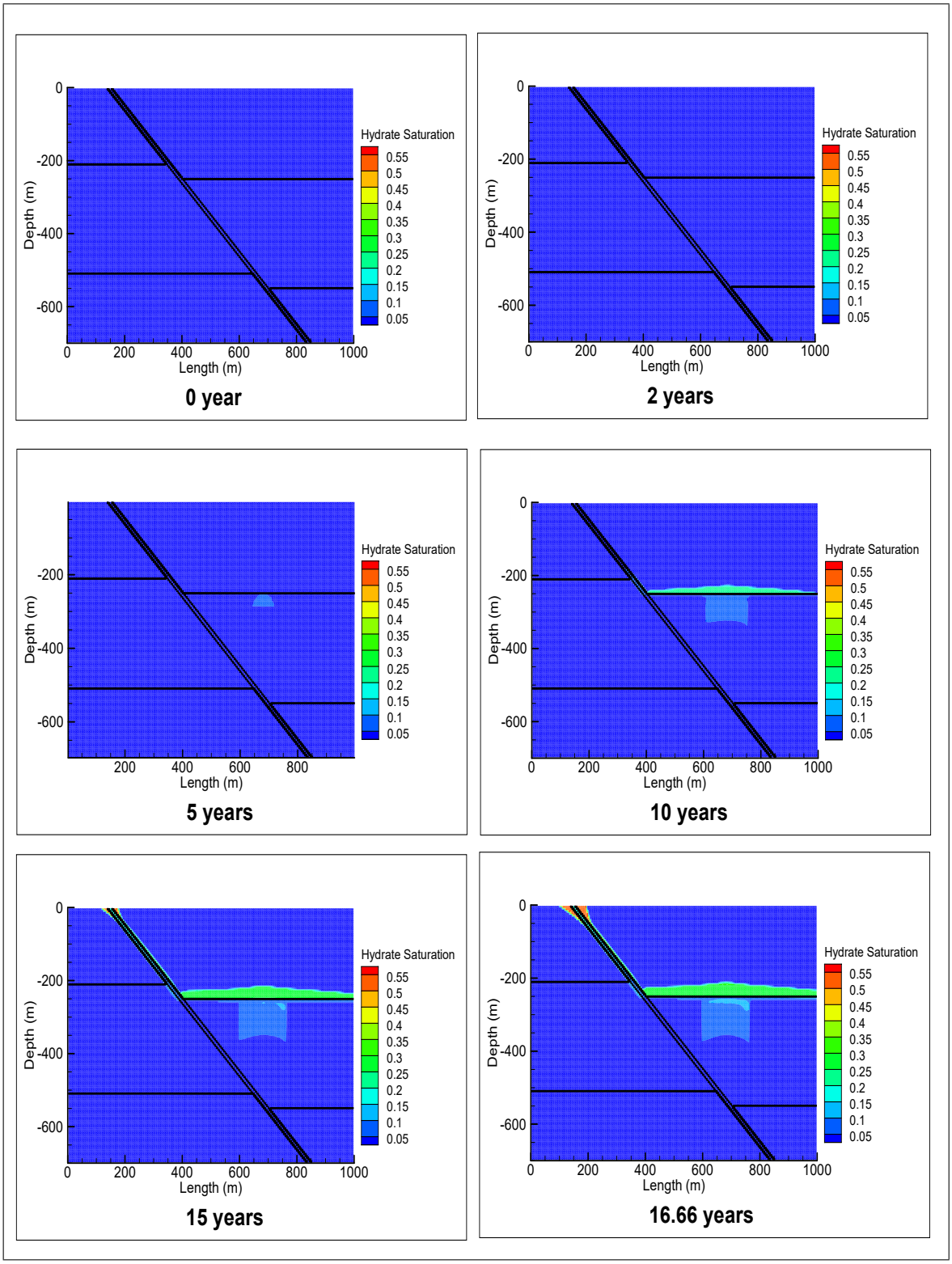

Figure 4.2: Basecase result: Hydrate saturation in the reservoir at different times

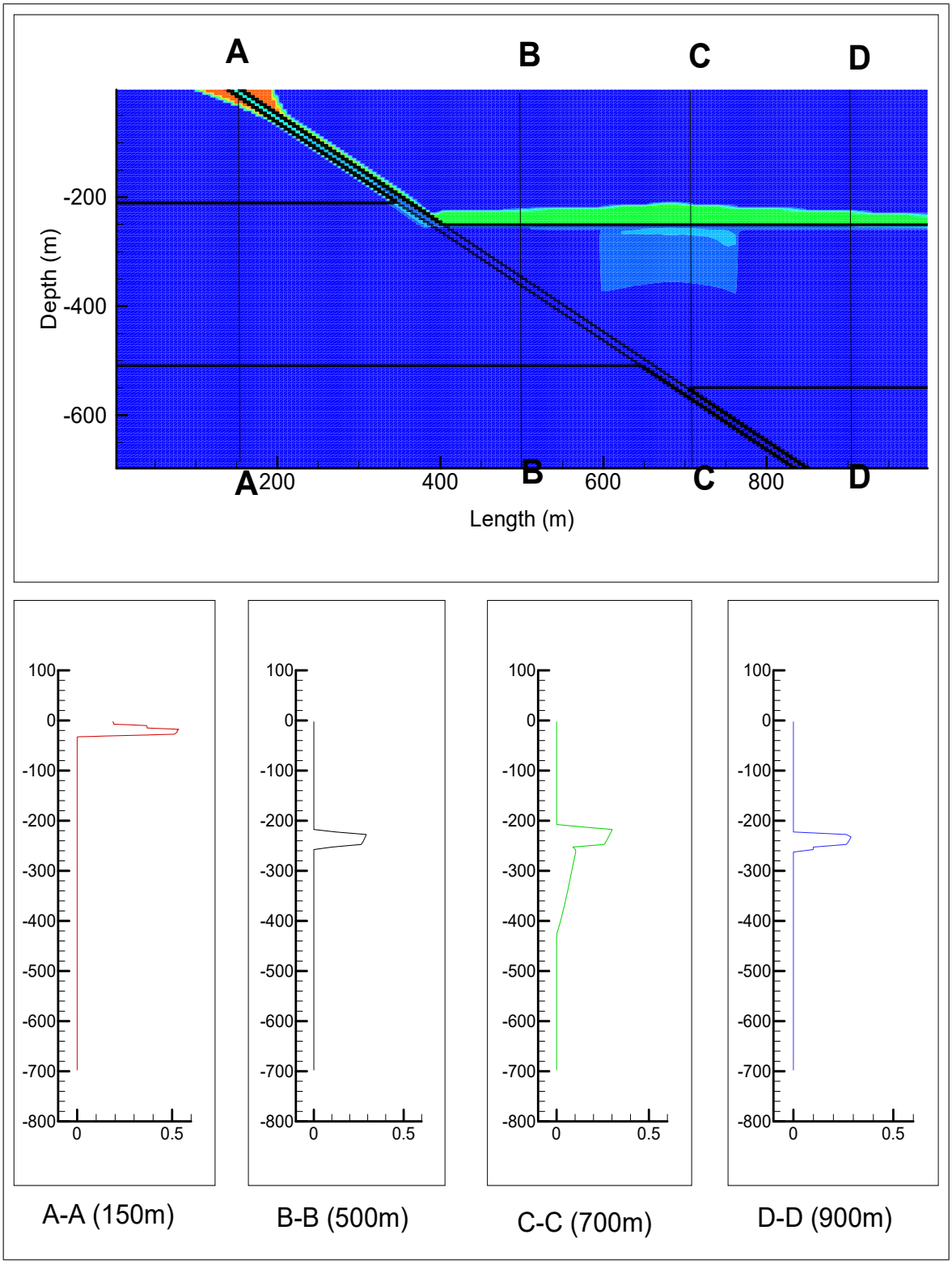

Figure 4.3: Basecase result: Depth vs Hydrate saturation in the reservoir at different vertical sections

As solid hydrates evolve and clog the pores of the reservoir rock, the permeability is decreased. The decrease in permeability is quantified as a variable that gives the multiple of permeability after hydrate formation (Figure 4.4). The variable can be from 0 to 1, where 0 is absolute clogging of pores so that the permeability is decreased to 0 while 1 is where there is no hydrate presence such that the permeability is decreased.

The stratigraphy of the basecase model generates a distinct hydrate body geometry. As evident by Figure 4.5, the gas moves up through the fault zone to enter the permeable sand layer and buoyancy drives the gas upwards within the sand zone. As the gas reaches the top of the sand zone, it starts to spread along the sand-shale boundary and continues to move upwards into the shale zone. The shale layer, having lower permeability than the underlying sand layer doesnt allow the gas to move as freely upwards as in the sand layer. Thus, the free methane gas moves sideways and also continues to move upwards through the fault zone. Due to the upthrow of 40m along the fault zone, the sand layer in the foot wall gets almost no gas flow since all the gas flows into the hanging wall sand layer.

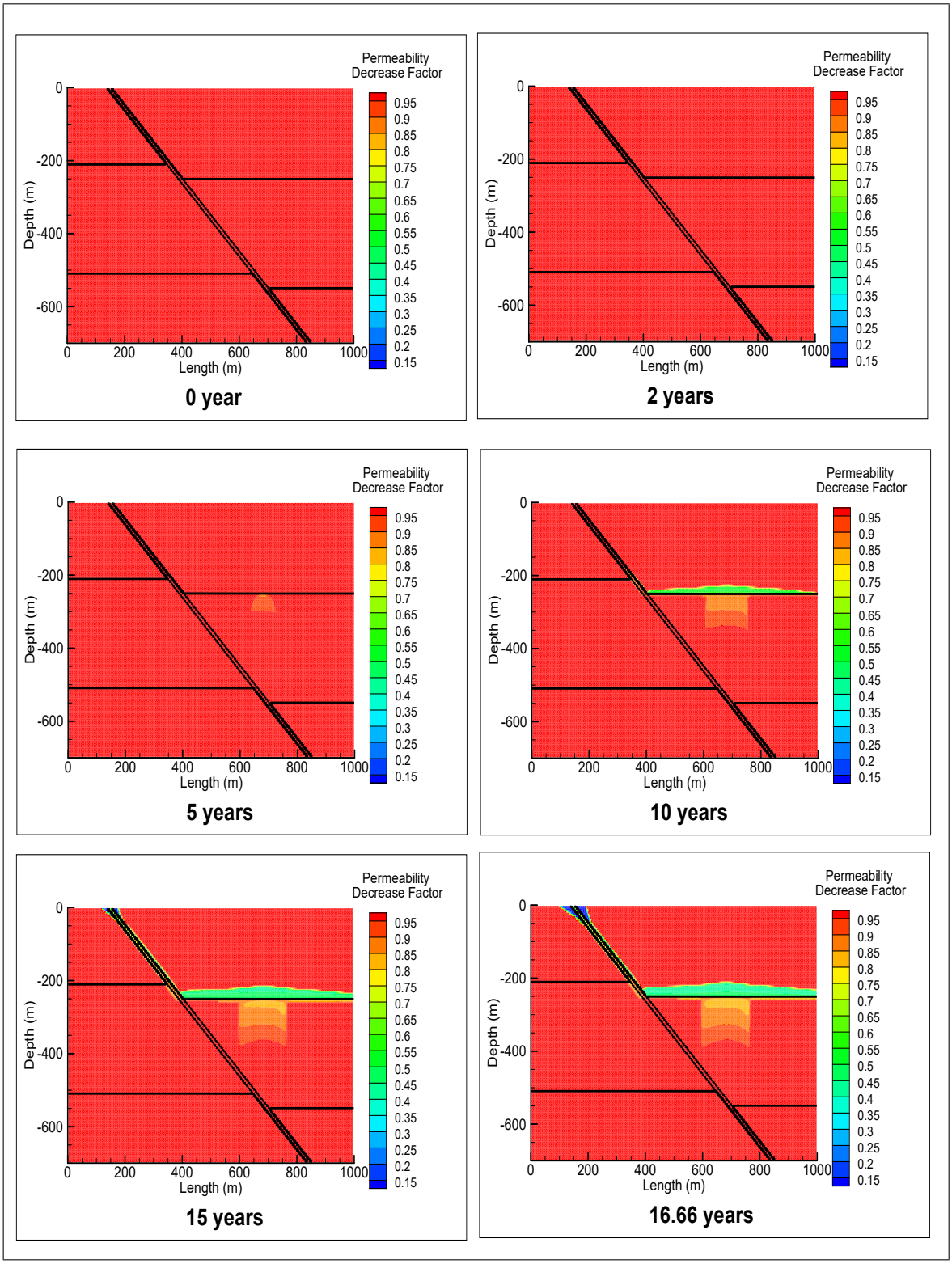

Figure 4.4: Basecase result: Permeability reduction factor in the reservoir at different times

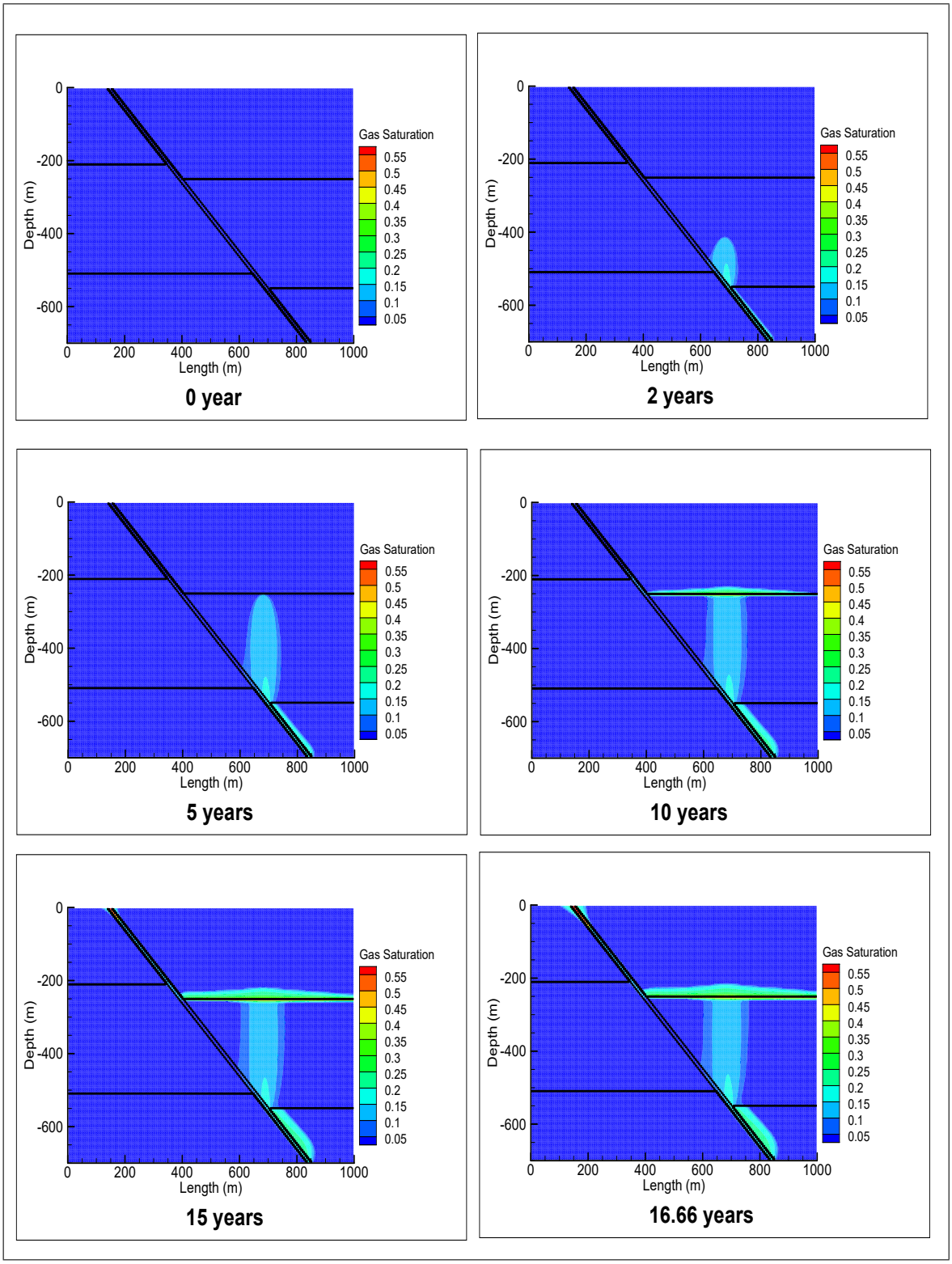

Figure 4.5: Basecase result: Free methane gas saturation in the reservoir at different times

Pressure in the reservoir increases as the fluid is injected and it dissipates across the length of the reservoir (Figure 4.6). As the gas migrating up through the fault is thermogenic in nature, it has higher heat content than the porewater in the reservoir and geothermic gradient is altered due to it. It is evident from Figure 4.7 that the temperature rises at regions where gas migration occur, which includes the migration path of the fault zone, sand layer and the overlying shale layer. It can also be inferred from the temperature distribution and hydrate saturation (Figure 4.2) that the higher temperature of the gas flowing up increase the reservoir temperature and the base of gas hydrate stability zone (BHSZ) is moved up. This explains the formation of hydrates in the sand layer in the beginning but as more heat is transferred from below, the base of hydrate stability zone moves upwards and into the shale layer. It has been previously established that the base of the hydrate stability zone (BHSZ) can move significantly with upward movement of hot fluids [61].

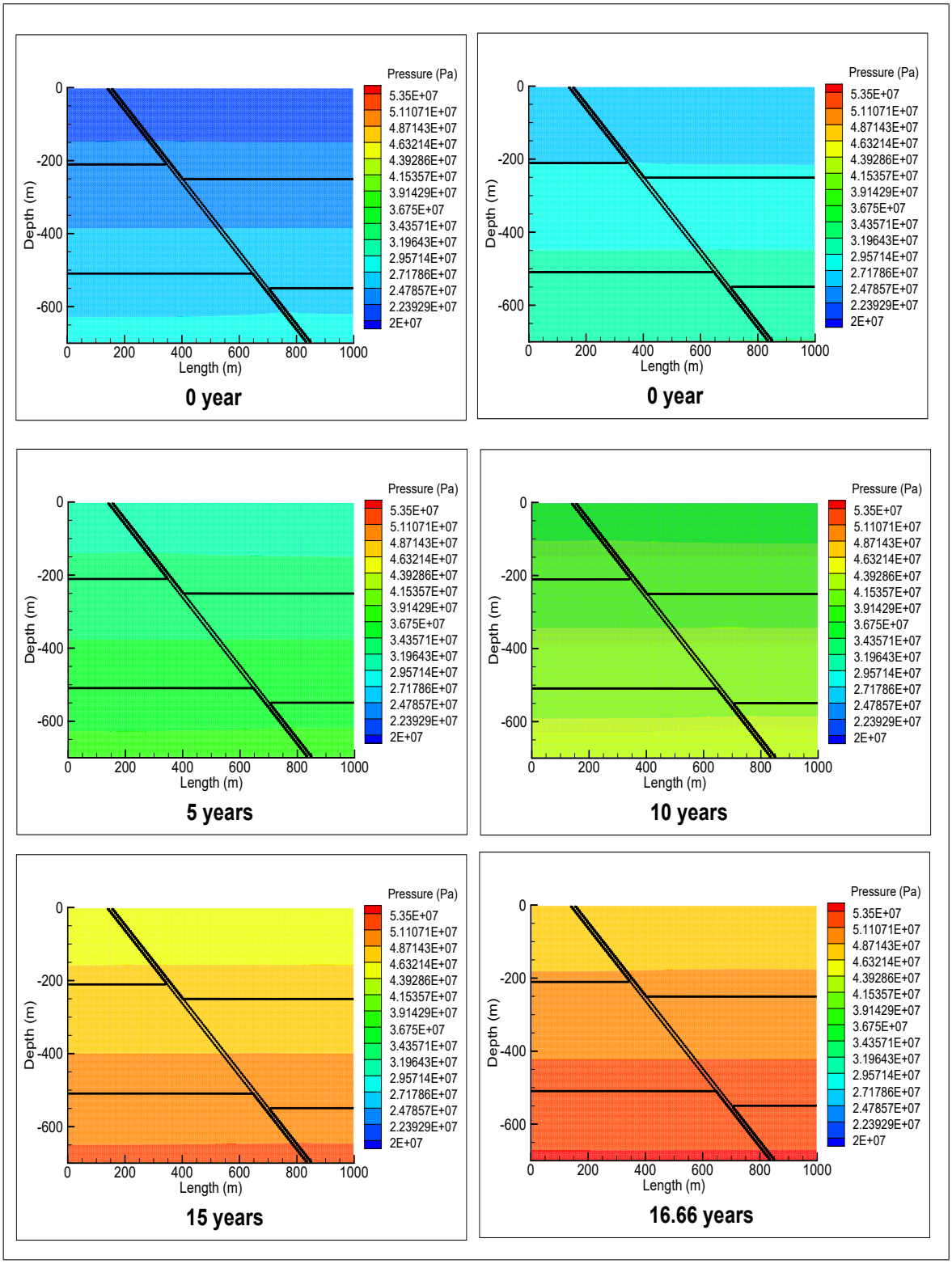

Figure 4.6: Basecase result: Pressure distribution in the reservoir at different times

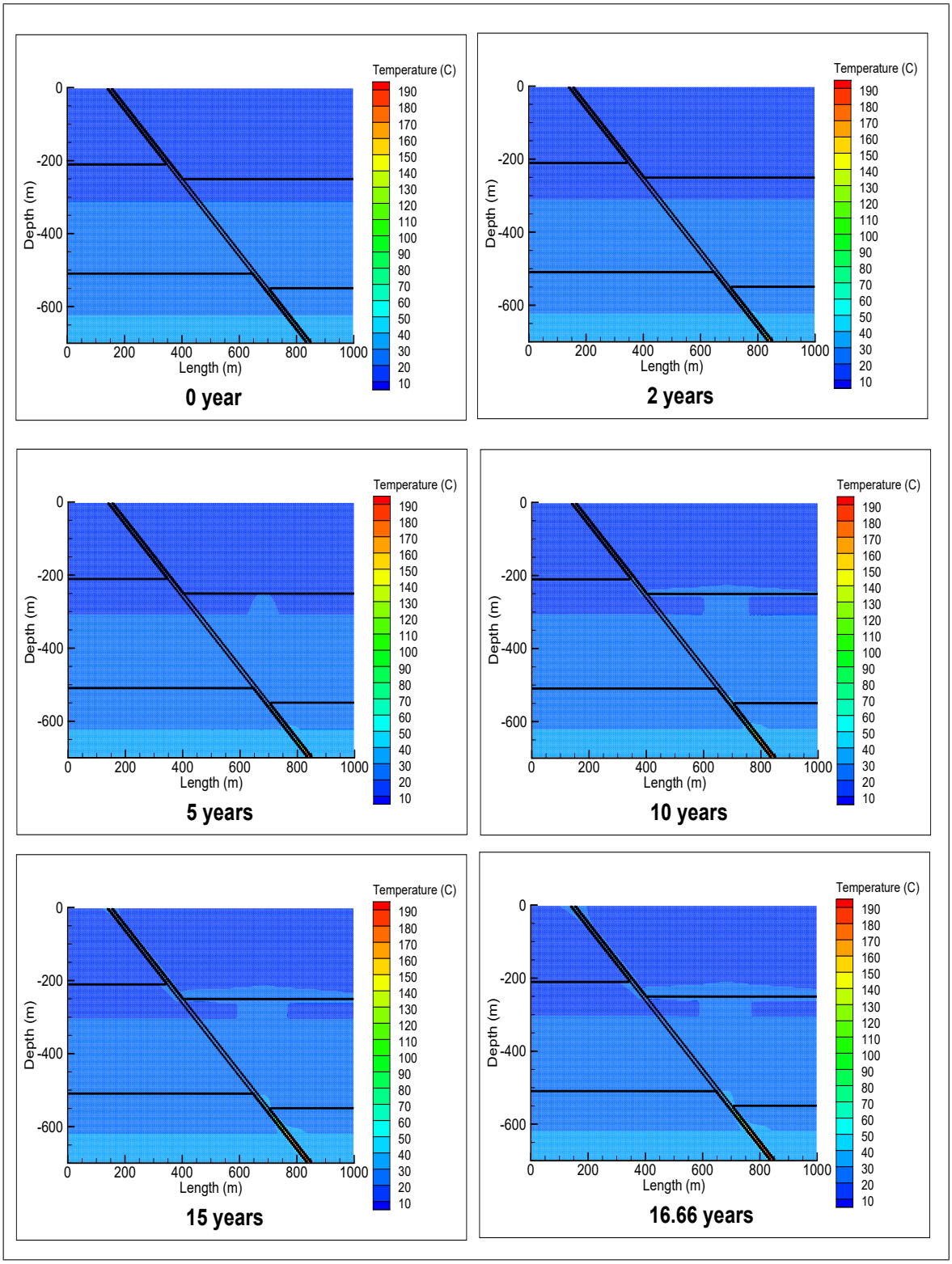

Figure 4.7: Basecase result: Temperature distribution in the reservoir at different times

4.2 Sensitivity Analyses Results

Sensitivity analyses were performed in order to further understand the impacts of different reservoir and flow parameters. Flow rate, fault angles, permeability, stratigraphy, boundary conditions and inhibitor concentrations are changed and results analyzed as follows.

4.2.1 Flow Rates

At different gas flow rates, the simulations ran for varying times and hydrates formation was much faster at higher rates. The mass of hydrates formed in the system is found to be highly dependent on the flow rate of free gas through the fault. A flowrate of 3E-4 kg/s produces a higher amount of hydrates (Figure 4.8) whereas lower flow rates of 3E-6 kg/s and 3E-7 kg/s do not yield any hydrate as the gas does not reach the hydrate stability zone, and the gas saturation is very low (Figure 4.9). Most of the gas that is injected is used up as soluble methane in the reservoir. While dissolved methane is also able to form hydrates under the right conditions, it does not reach hydrate stability zone in 500 years in order to form hydrates. Flow rate of thermogenic methane gas through the fault depends on the methane generation rate, amount and fault activation period. This research shows that at different flow rates, the methane hydrate generation differ and the exact estimation of hydrate reserves can be determined only by having a strong understanding of the methane gas flow.

Like the gas saturation, the distribution of hydrate saturation varies with flow rates of methane gas (Figure 4.10). The hydrate geobody is the largest with highest accumulation of hydrates at 6.15E6 kg of hydrates which is equivalent to 1 million cubic meters of free gas when the flow rate is 3E-4kg/s. This volume estimate is in alignment with the seismic estimation in the Green Canyon region in the Gulf of Mexico [23]. The majority of methane hydrates present in the model is at the shale layer of the hanging wall which

can be attributed to the flow of gas into the shale layer where hydrate stability condition is reached. High saturation of methane hydrates in the shale zone rather than the sand layer is from the flow of gas into the shale zone from sand zone due to buoyancy. Initial hydrate formation in the sand zone is replaced by gas as the hot gas is known to push the base of the hydrate stability zone [61].

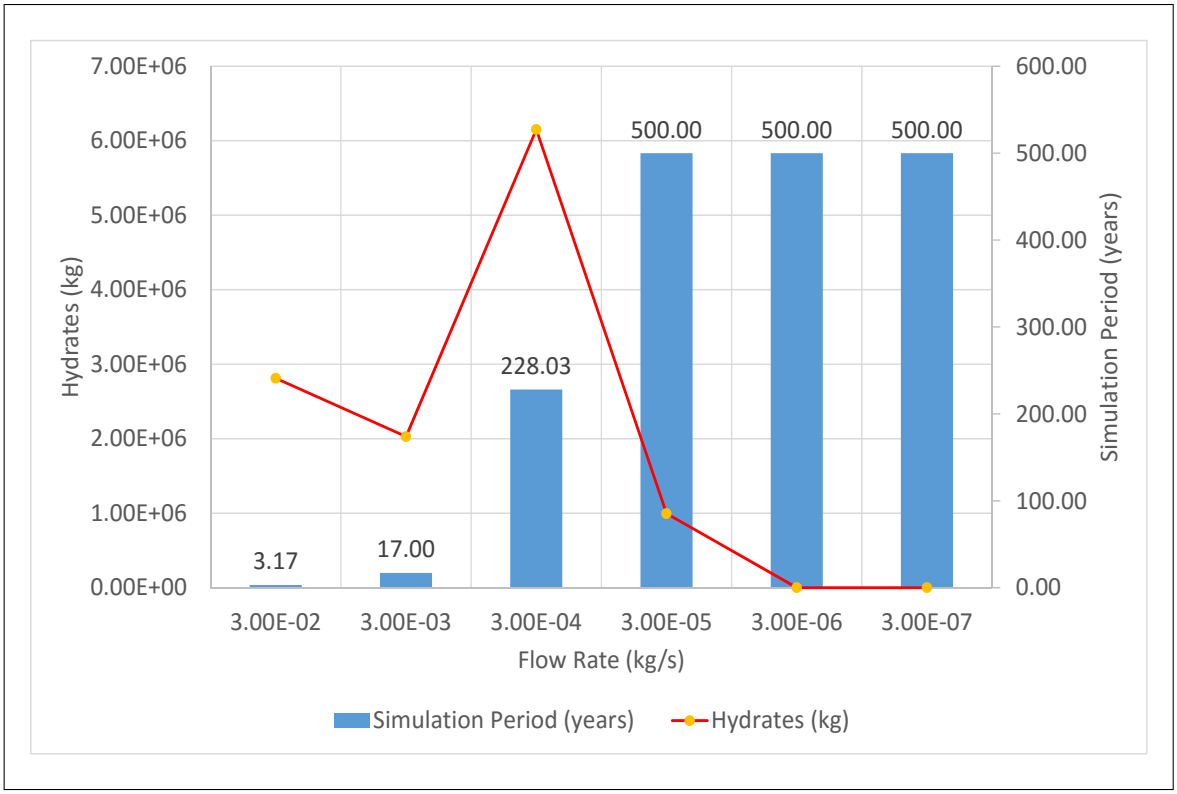

Figure 4.8: Effect of flow rate of methane gas on the simulation time and total hydrates in the system

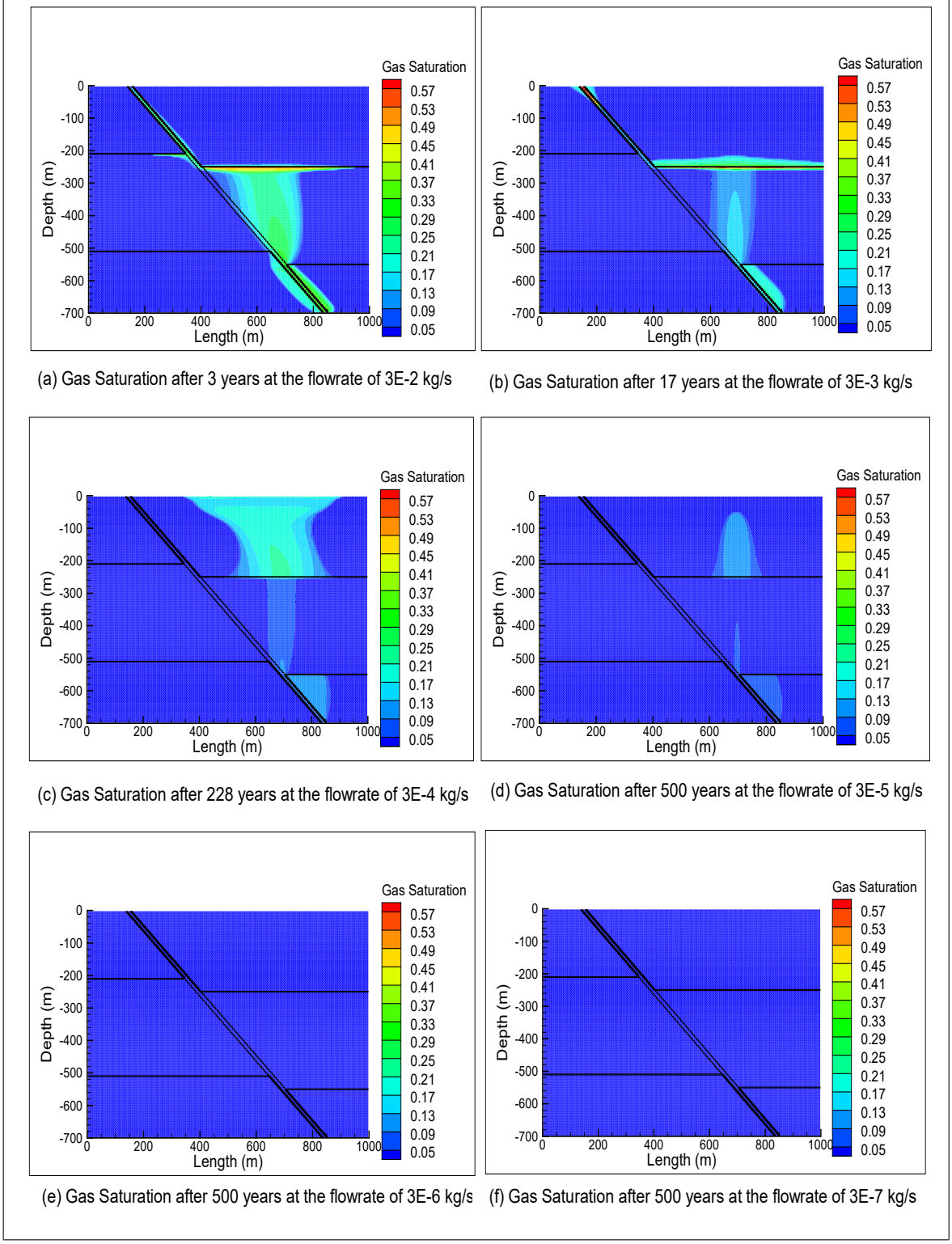

(a) Gas Saturation after 3 years at the flowrate of 3E-2 kg/s

(b) Gas Saturation after 17 years at the flowrate of 3E-3 kg/s

(c) Gas Saturation after 228 years at the flowrate of 3E-4 kg/s

(d) Gas Saturation after 500 years at the flowrate of 3E-5 kg/s

(e) Gas Saturation after 500 years at the flowrate of 3E-6 kg/s

(f) Gas Saturation after 500 years at the flowrate of 3E-7 kg/s

Figure 4.9: Free gas saturation at the end of simulation time for different flow rates

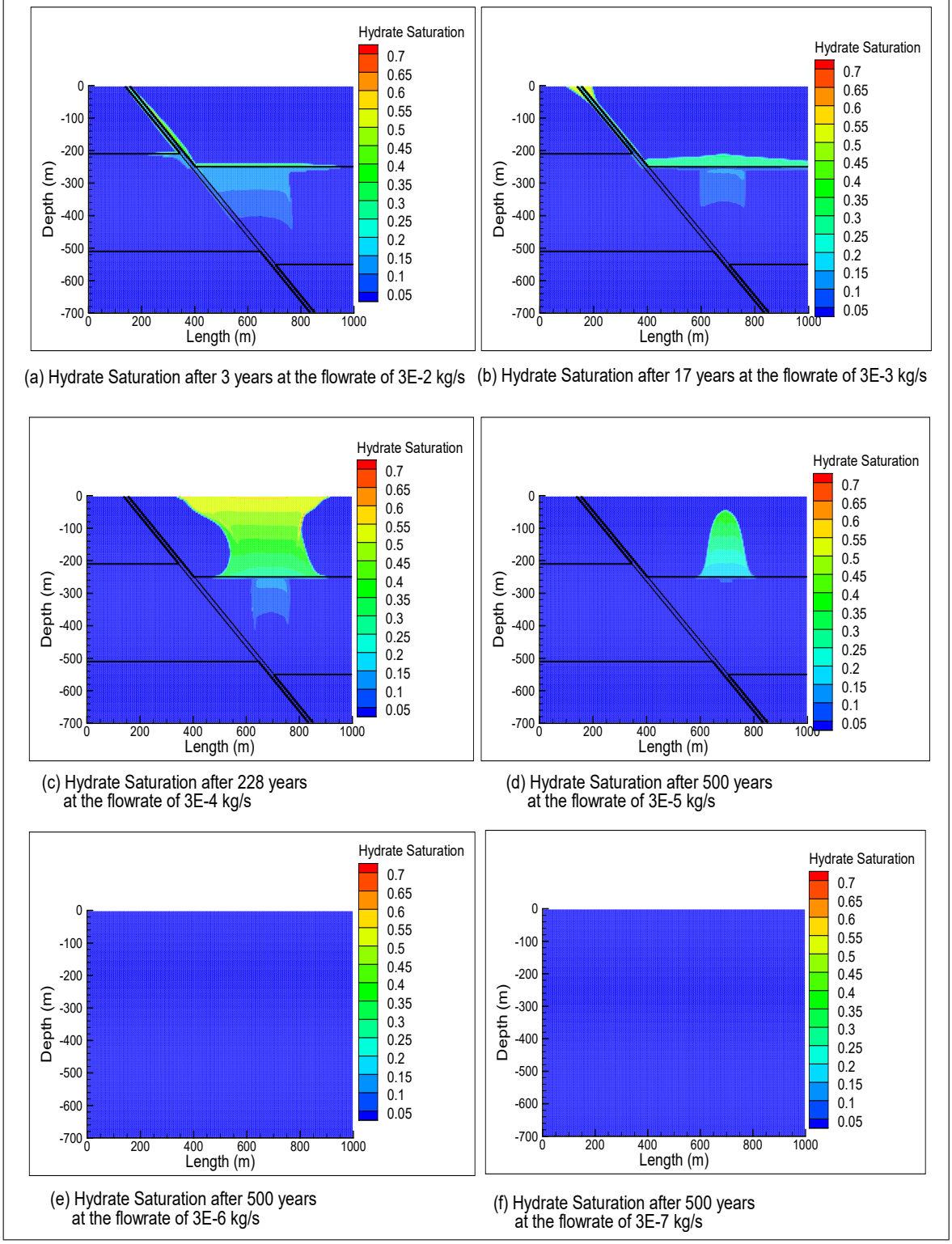

(a) Hydrate Saturation after 3 years at the flowrate of 3E-2 kg/s

(b) Hydrate Saturation after 17 years at the flowrate of 3E-3 kg/s

(c) Hydrate Saturation after 228 years at the flowrate of 3E-4 kg/s

(d) Hydrate Saturation after 500 years at the flowrate of 3E-5 kg/s

(e) Hydrate Saturation after 500 years at the flowrate of 3E-6 kg/s

(f) Hydrate Saturation after 500 years at the flowrate of 3E-7 kg/s

Figure 4.10: Hydrate saturation at the end of simulation time for different flow rates

The simulation was slower for higher flow rates and with only 72 hours available at the High Performance Computing center at LSU, the simulation time was significantly low for higher flow rates of methane gas. The simulation was run for 500 years and only three simulations with lowest rates of flow ran for the full 500 years in the available 72 hours. It can be attributed to faster hydrate formation in the system, which means that the primary variable switching used in the TOUGH+HYDRATE code finds it harder to converge with larger time steps. Therefore, the code automatically decreases the time step size for convergence and thus the simulation runs slower.

4.2.2 Boundary Conditions

Boundary conditions of the reservoir also determine the flow of gas and in turn the formation and accumulation of methane hydrates. The base case model has a special case of Neumann boundary condition with zero flux at all sides, i.e. no flow. Thus the flow into the reservoir is conserved within the reservoir. For different reservoir types, the boundary conditions are different depending on surrounding rock properties, structure and stratigraphy. Three different conditions are tested with Dirichlet boundary (fixed pressure and temperature) at the top, sides and both to mimic large reservoirs or continuous geologic sequences. The resulting hydrate accumulations for these conditions are all different from the base case model. It is observed that for Dirichlet boundaries at the top and sides, hydrate accumulation is the highest (Figure 4.11).

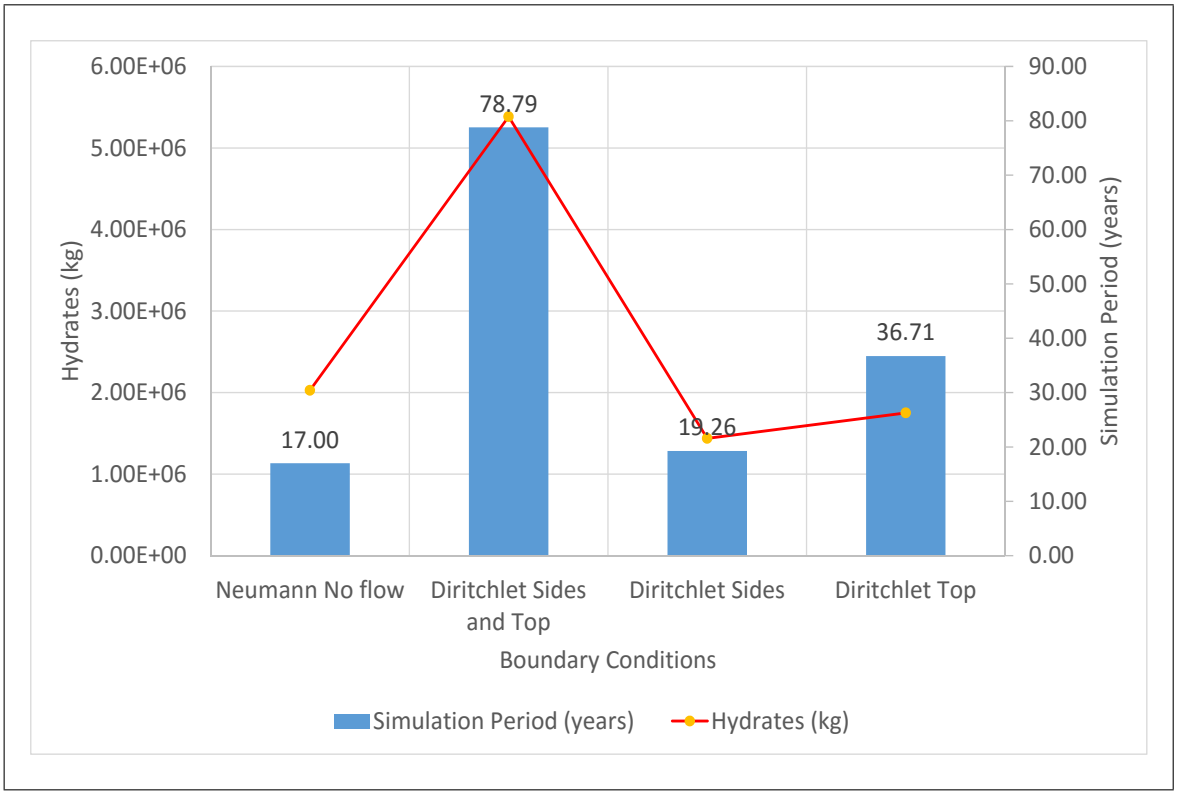

Figure 4.11: Effect of boundary conditions on the simulation time and total hydrates in the system

The gas saturation in the reservoir suggests that having constraining boundaries and continuous domains have distinct impact on gas flow (Figure 4.12). Gas saturation increased in the shale zone when the boundary conditions were changed from the base case model (no-flow). When the top boundary was continuous, the gas flow through the fault was increased while having continuous domain on the sides increased the lateral flow of gas. It can be concluded that a continuous domain or a large reservoir will have a larger spatial distribution of gas compared to a confined domain where gas tends to accumulate at a few favorable locations.

Since gas flow into the hydrate stability zone is a deciding factor for hydrate formation, hydrate formation followed the gas accumulation pattern. In reservoirs with continuous domains, the hydrate formation was more spatially distributed compared to the confined reservoir (Figure 4.13). The continuous domain allowed the gas to flow freely within the

reservoir and into the hydrate stability zone. While the highest hydrate saturation in the reservoir is observed when there is a no flow boundary (55%) and the lowest saturation when there is a continuous boundary (27%), there was greater spatial extent and higher mass of hydrates in the reservoir in the latter. Despite having a high spatial extent, the footwall received almost no hydrates as the driving mechanism is dominated by buoyancy in all cases. It can be inferred from this result that boundary condition is a dominant factor in determining the extent and concentration of hydrate geobody.

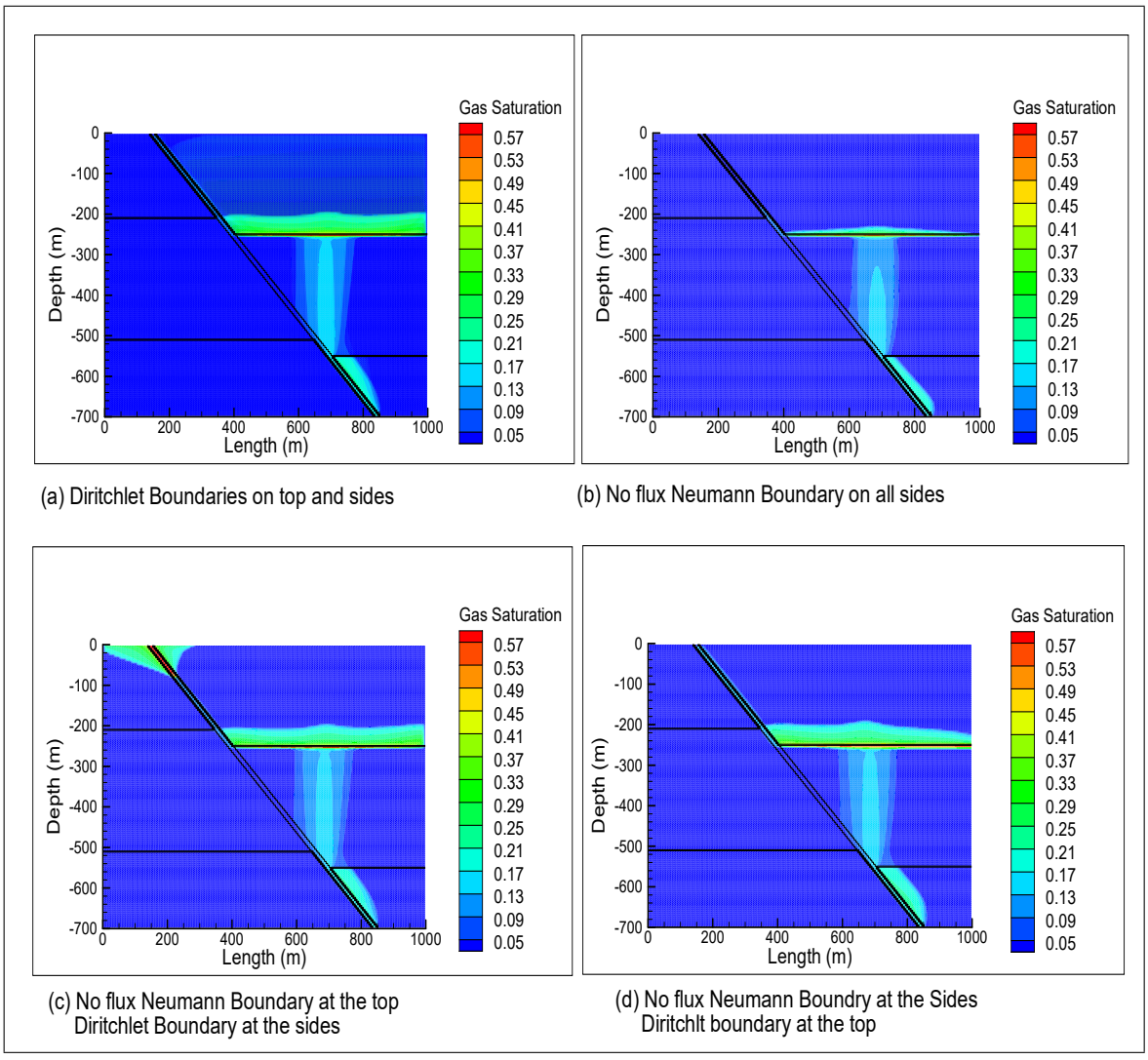

Figure 4.12: Gas saturation at the end of 17 years for different boundary conditions

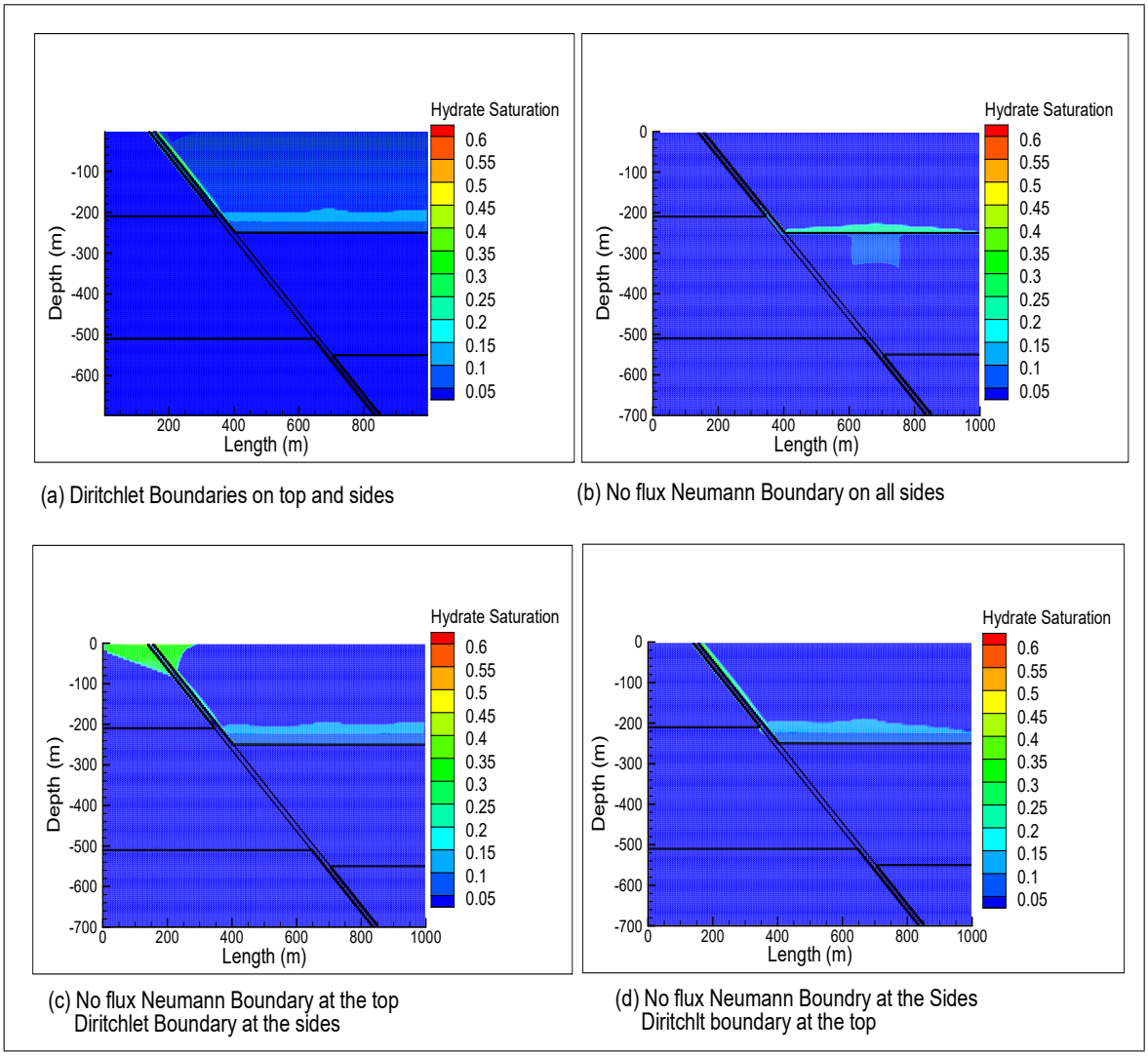

Figure 4.13: Hydrate saturation at the end of 17 years for different boundary conditions

4.2.3 Fault Angles

Fault angles differ in nature according to the stress condition of a particular location. Flow of gas and thus formation of hydrates also differ with different fault angles since the length of the flow path is different. Variation in the fault angle has an impact in the hydrate accumulation and the simulation time (Figure 4.14).

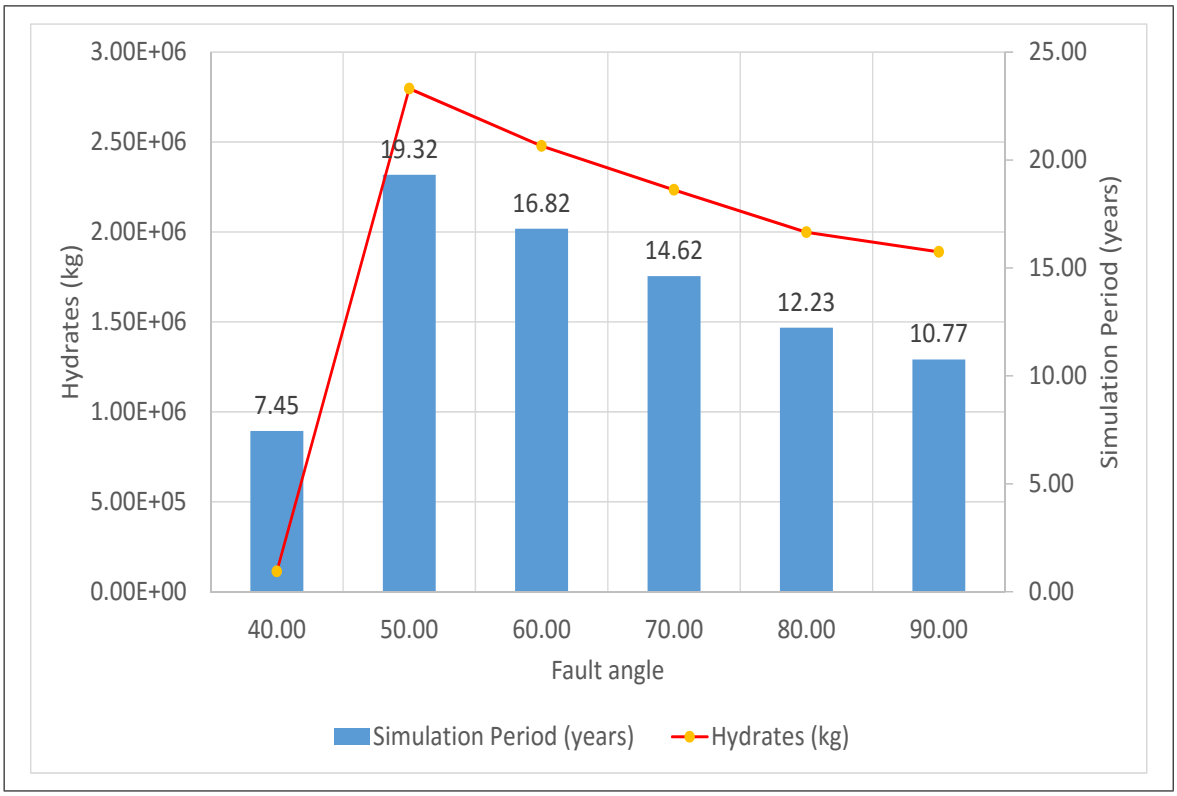

Figure 4.14: Effect of fault angle on hydrate formation

Simulation results at the end of 10 years were compared in order to observe the distribution of gas saturation (Figure 4.15). The gas saturation ranges were similar in all the cases with highest saturation values at about 60%. However, the distribution of gas in the reservoir varied when fault angle was steeper leading to higher gas and thus solid hydrates in the reservoir. Steeper faults also meant easier flow of gas in the fault zone due to buoyancy, and gas chimneys formed around the fault zones (Figure 4.15).

Hydrate saturation also followed the same pattern with hydrates forming inverted Christmas tree structures at the top of steep faults (Figure 4.16). For the 40^0 fault, the hydrate formation was negligible as the gas could not migrate to the gas hydrate stability zone. The accumulation pattern of hydrates along the top of the model at the sea floor indicates that there may be mounds of hydrates on the surface as corroborated by field observations in marine hydrates [33]. The maximum gas hydrate saturation in the cases with fault angles higher than 50^0 are about 50% with most accumulated at the top of the reservoir for steep faults. Production planning from hydrates must take the fault angle into consideration while estimating the hydrate reserve, its location and well placement.

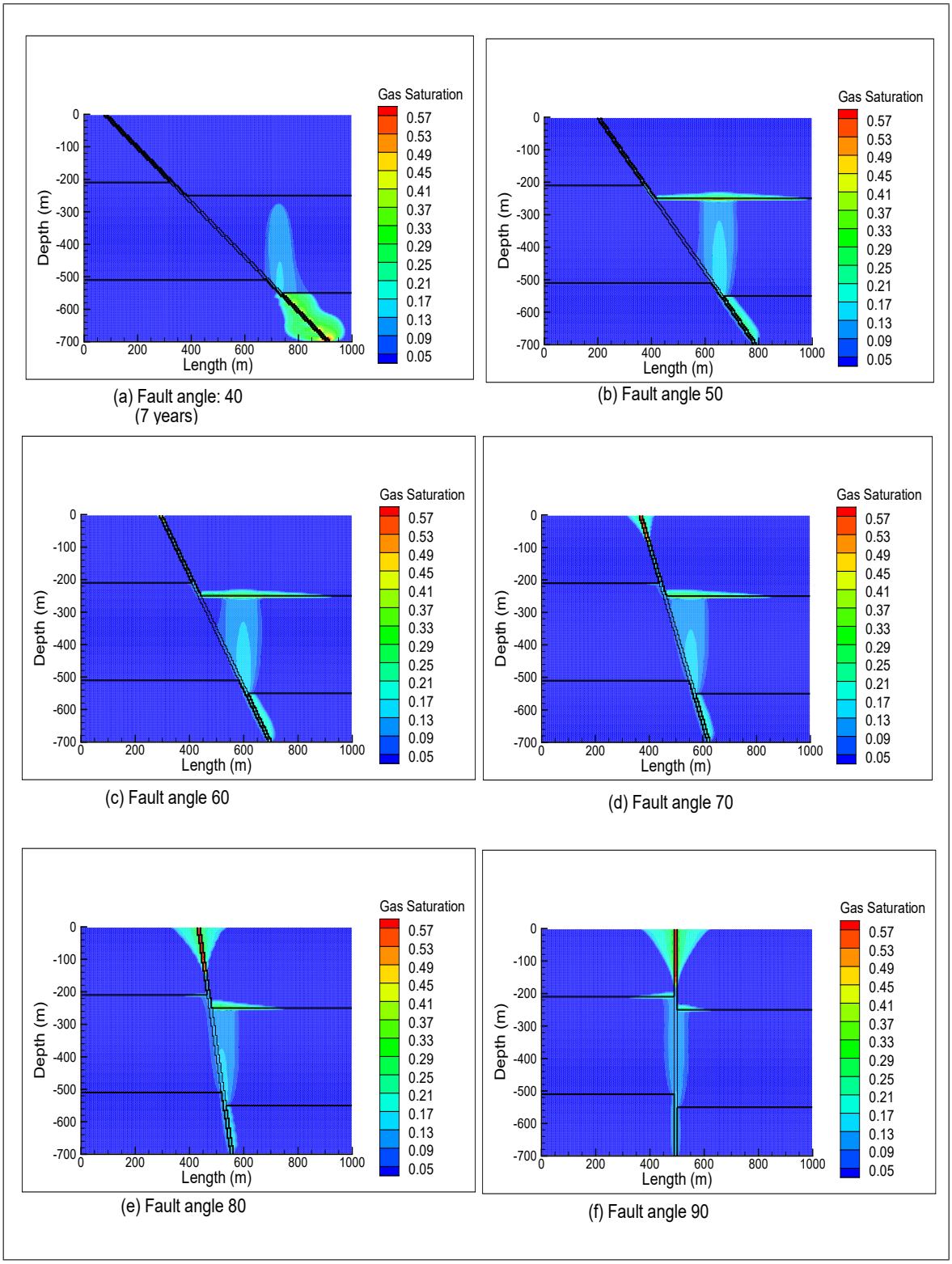

Figure 4.15: Gas saturation at the end of 10 years for different fault angles

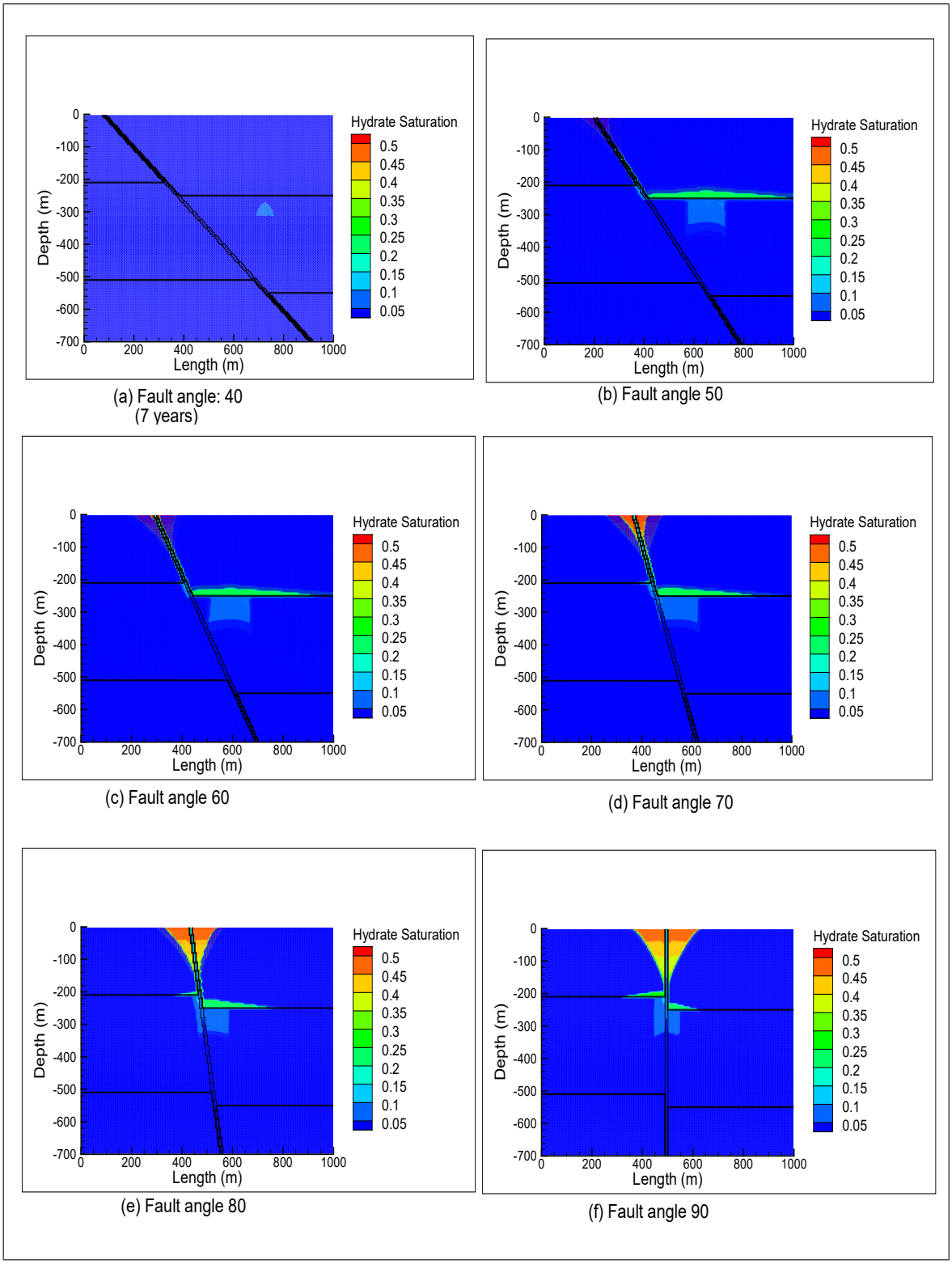

Figure 4.16: Hydrate saturation at the end of 10 years for different fault angles

4.2.4 Permeability

Permeability of rock is the ability of a fluid to flow through it due to connectivity of the pores. As permeability is changed, the ability of the fluid phase to flow through the rock is changed. Vertical gas migration through the sand and shale layers was observed in the base case model and therefore the permeability of each layer is changed by an order of magnitude from the base case model (Table 4.1).

Table 4.1: Permeability values used in different rock types for sensitivity study

SN	Rock Type	Description	Permeability
1	Sand	High	1E-11 m^2 (H) 1E-12 m^2 (V)
2	Sand	Low	1E-13 m^2 (H) 1E-14 m^2 (V)
3	Shale	Low	1E-16 m^2 (H) 1E-17 m^2 (V)

Figure 4.17 shows the comparison of gas hydrate accumulation and the simulation periods for different permeability values.

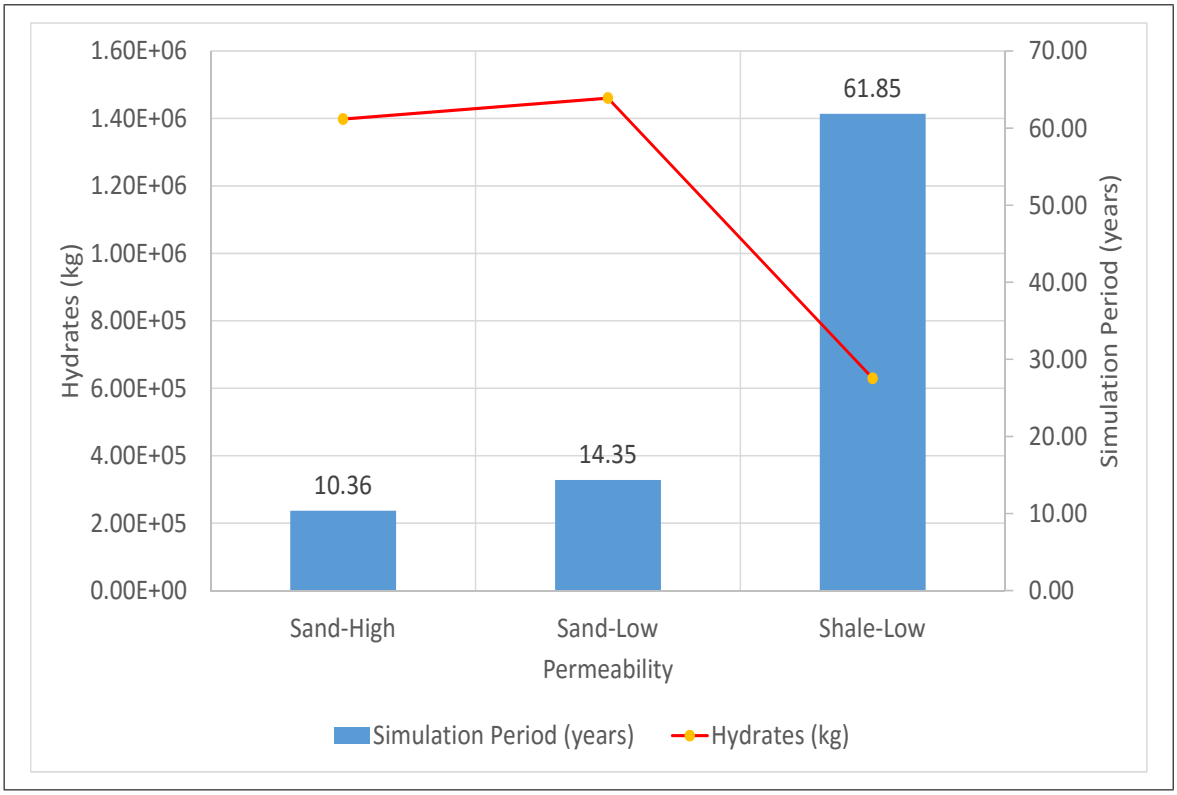

Figure 4.17: Effect of permeability of sand and shale on the simulation time and total hydrates in the system

Gas saturations were compared at the end of 10 years of simulation (Figure 4.18) which demonstrates that the gas migration through the sand zone vertically is inhibited in a low permeability sand zone. It can also be inferred that in the absence of a highly permeable sand zone, the gas migration is mainly along the fault as seen in the low permeability sand. The flow of gas into the shale zone is also reduced with reduced shale permeability and the gas tends to accumulate at the base of the shale layer.

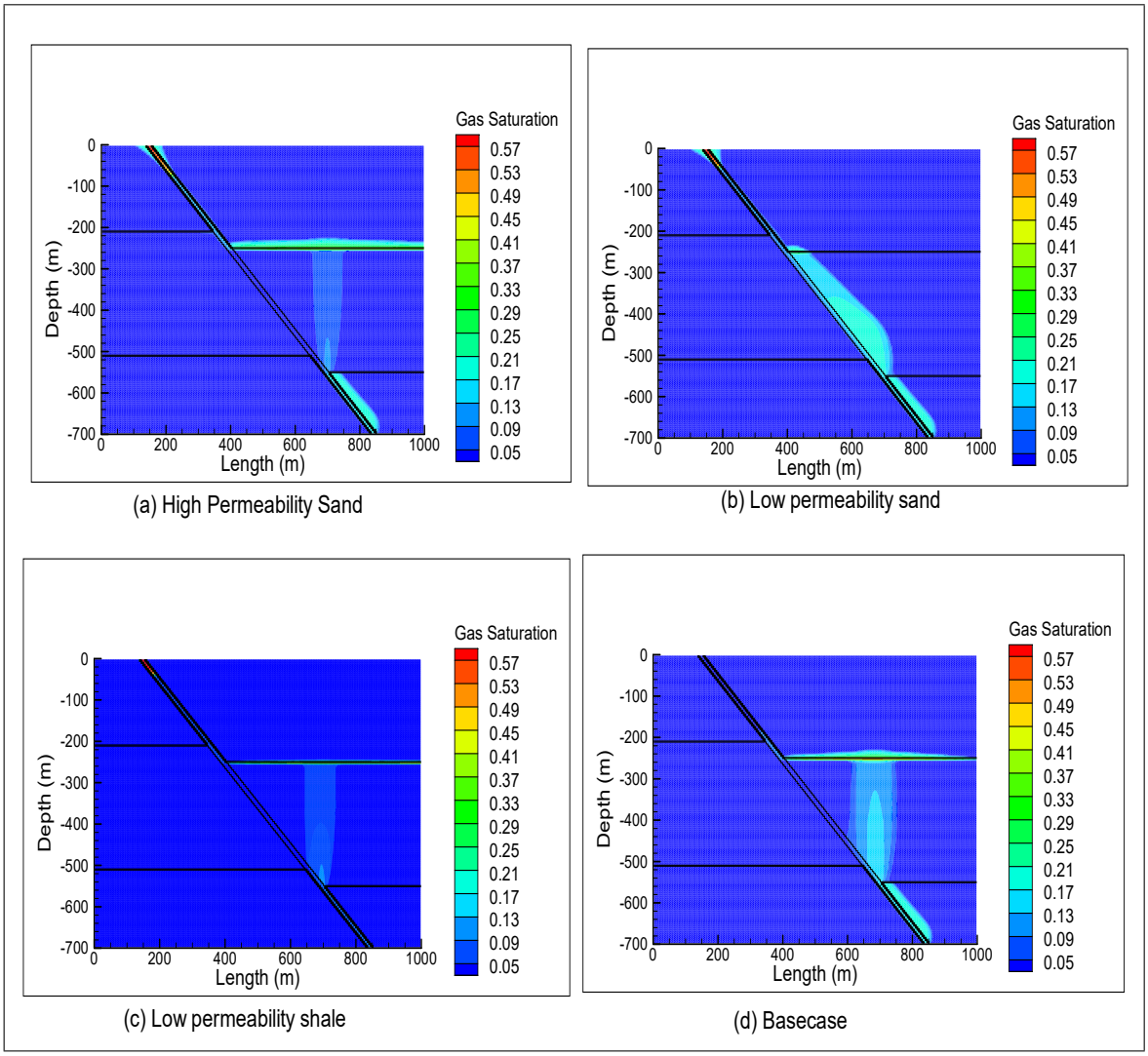

Figure 4.18: Gas saturation at the end of 10 years for different permeability values

Hydrate saturation distribution, like gas saturation also differs with different permeability values (Figure 4.19). Although the highest hydrate saturation is about 50% in all cases, highly permeable sand facilitates the gas movement to the hydrate stability zone and hydrate concentration at the shale zone and the fault zone increases. Faster migration of gas into the hydrate stability zone also allows the hydrates to spread laterally and along the fault. Lower permeability of sand zone forces the gas to flow through the fault zone and hydrate accumulation is concentrated along the fault with very little hydrates laterally spread along the base of the shale layer as seen in other cases. It also indicates that in reservoirs with low permeability on all strata, the hydrates are mostly formed along the

fault. It is a scenario where production from hydrates would be difficult as there would not be enough hydrate in the main reservoir. However, the hydrate content is higher along and near the fault zone.

For low permeability shale layer, the gas cannot flow through it easily and hydrate formation is inhibited since the gas cannot reach the hydrate stability zone. It may prove to be a favorable case for the production scenario if the hydrate stability condition is reached in the reservoir below the fault zone as the shale would act as a seal rock.

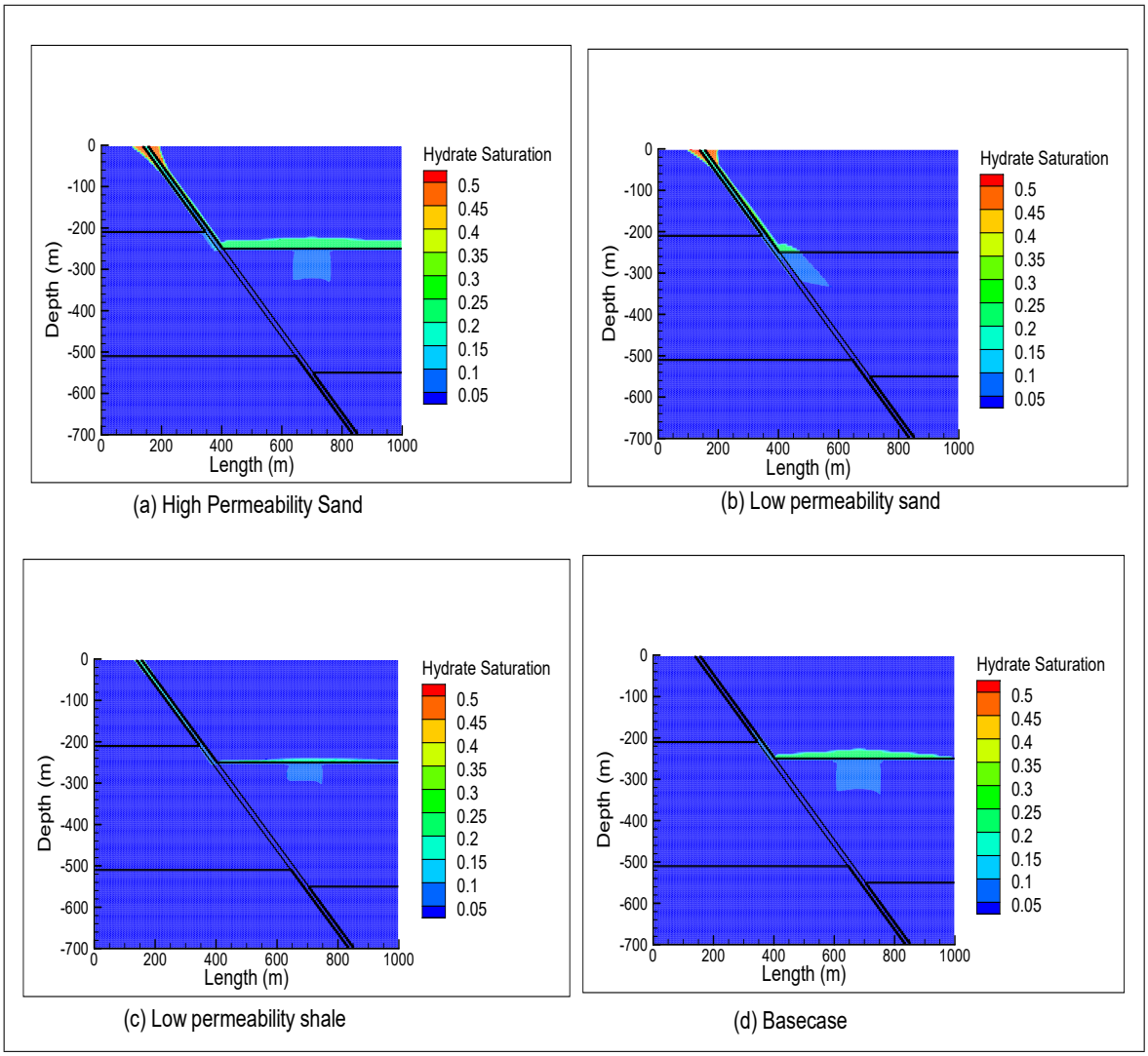

Figure 4.19: Hydrate saturation at the end of 10 years for different permeability values

4.2.5 Inhibitors

Hydrate formation in marine sediments is affected by the presence of salt, which acts as an inhibitor to hydration. The average salinity of Gulf of Mexico of 3.5% was used to study the effect of inhibitor and it was observed that hydrate formation is decreased by the salinity. Figure 4.20 shows the total hydrate accumulation and the simulation years.

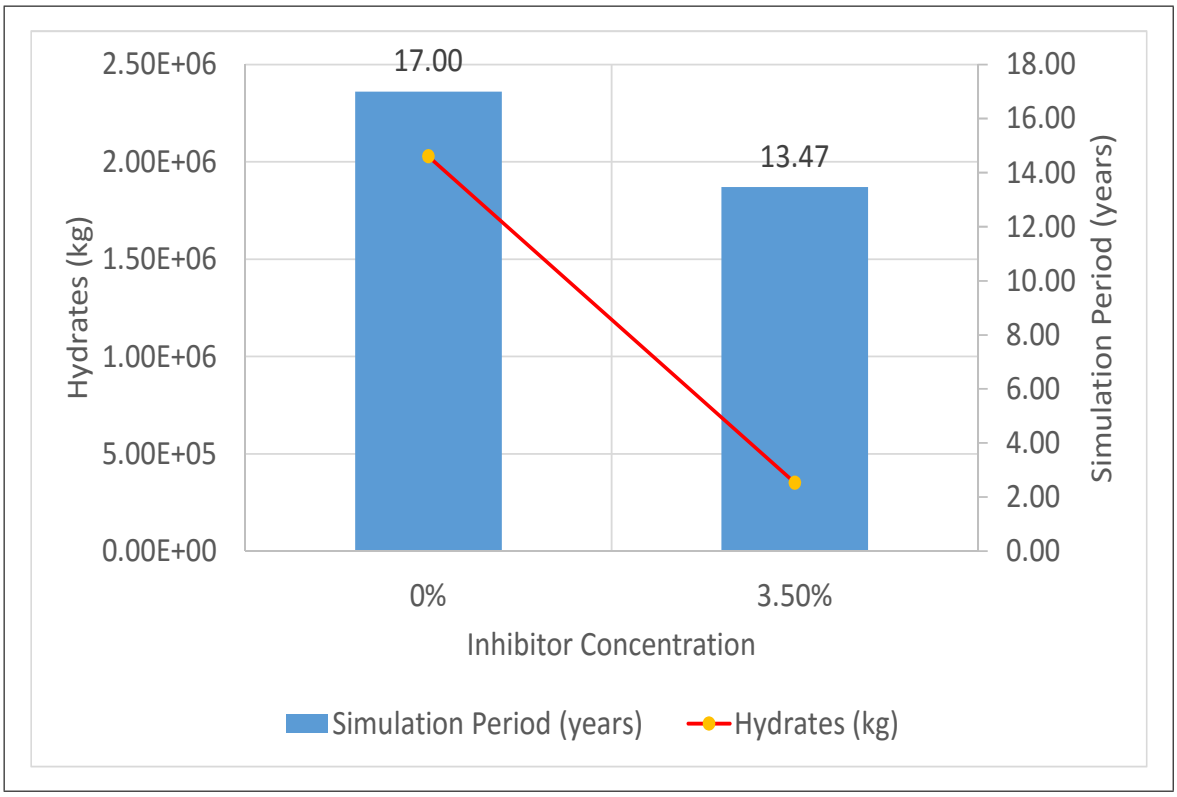

Figure 4.20: Effect of inhibitor (salt) on the simulation time and total hydrates in the system

The introduction of salinity in the pore water of the reservoir has a visible impact on the gas and hydrate saturation (Figure 4.21). While the flow of gas is almost identical in nature, the formation of hydrates is decreased in the case with the inhibitor (salt). The highest hydrate saturation in the reservoir is decreased from 25% to 10%. The result confirms the inhibition effect of salinity in the hydrate stability condition in the reservoir [17]. Reservoir characterization of hydrate reserves must take into account the field data of the pore water salinity in order to accurately estimate the quantity and saturation of hydrates.

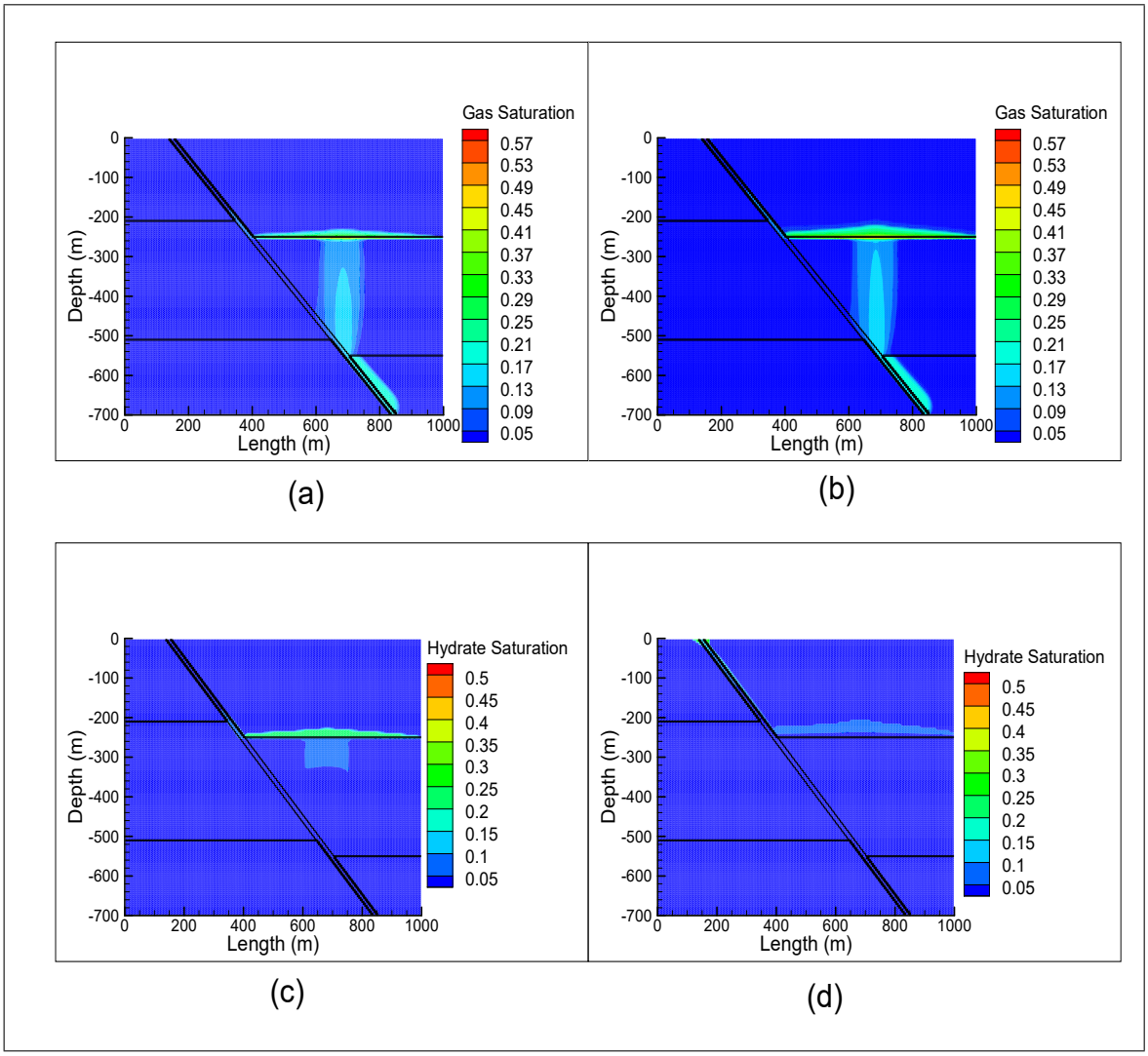

Figure 4.21: Free gas and hydrate saturations after 10 years. (a) Free gas saturation with no inhibitor, (b) Free gas saturation with inhibitors, (c) Hydrate saturation without inhibitor, (d) Hydrate saturation with inhibitors

4.2.6 Stratigraphy

Hydrate formation depends upon the rock properties, and geometry of the formations in the gas hydrate stability zone. In this research, the thickness of the sand layer is changed to observe the gas flow and hydrate formation. The gas flow rate is taken as 3E-4 kg/s in order to simulate for a longer period of time. Three cases of sand layer thickness are simulated with 100m, 200m and 400m thick sand layers. The results are compared with

the base case result of 300m thick sand. Figure 4.22 shows the simulation period and total hydrate accumulation in each case. It is observed that the simulation period as well as the hydrate accumulation increases with the increase in the sand thickness up to 300m thick sand and decreases slightly in the 400m thick sand. It may be due to slower flow of gas into the gas hydrate stability zone.

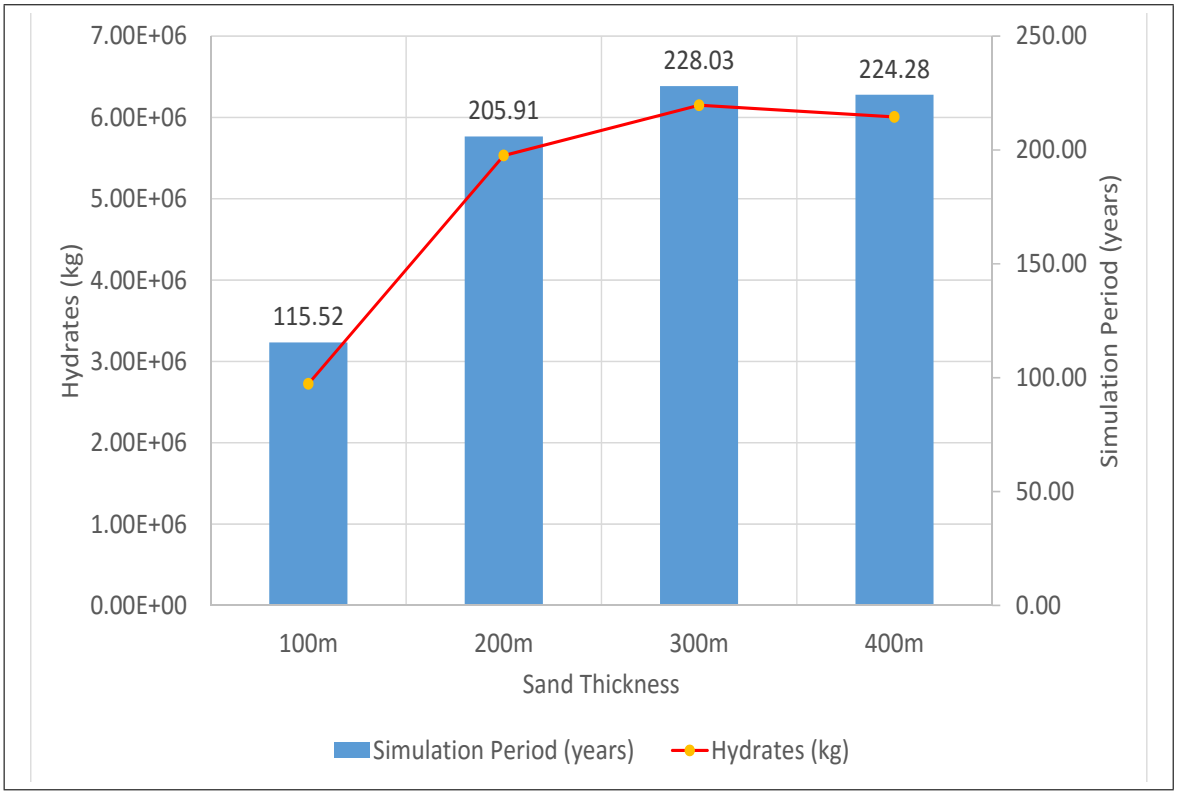

Figure 4.22: Effect of stratigraphy on the simulation time and total hydrates in the system

Free gas saturation in the reservoir after 100 years indicate that flow through the sand zone plays a major role in the migration into the gas hydrate stability zone (Figure 4.23). It is seen that the gas flow initiates at the fault zone but once it reaches the sand layer, it rises vertically due to buoyancy. The gas reaches the shale layer directly above the point where the fault intersects the sand layer at the bottom. Apart from the location of the gas accumulation, there is not much difference in the four cases with similar amount and maximum saturation of gas remaining at 22%.

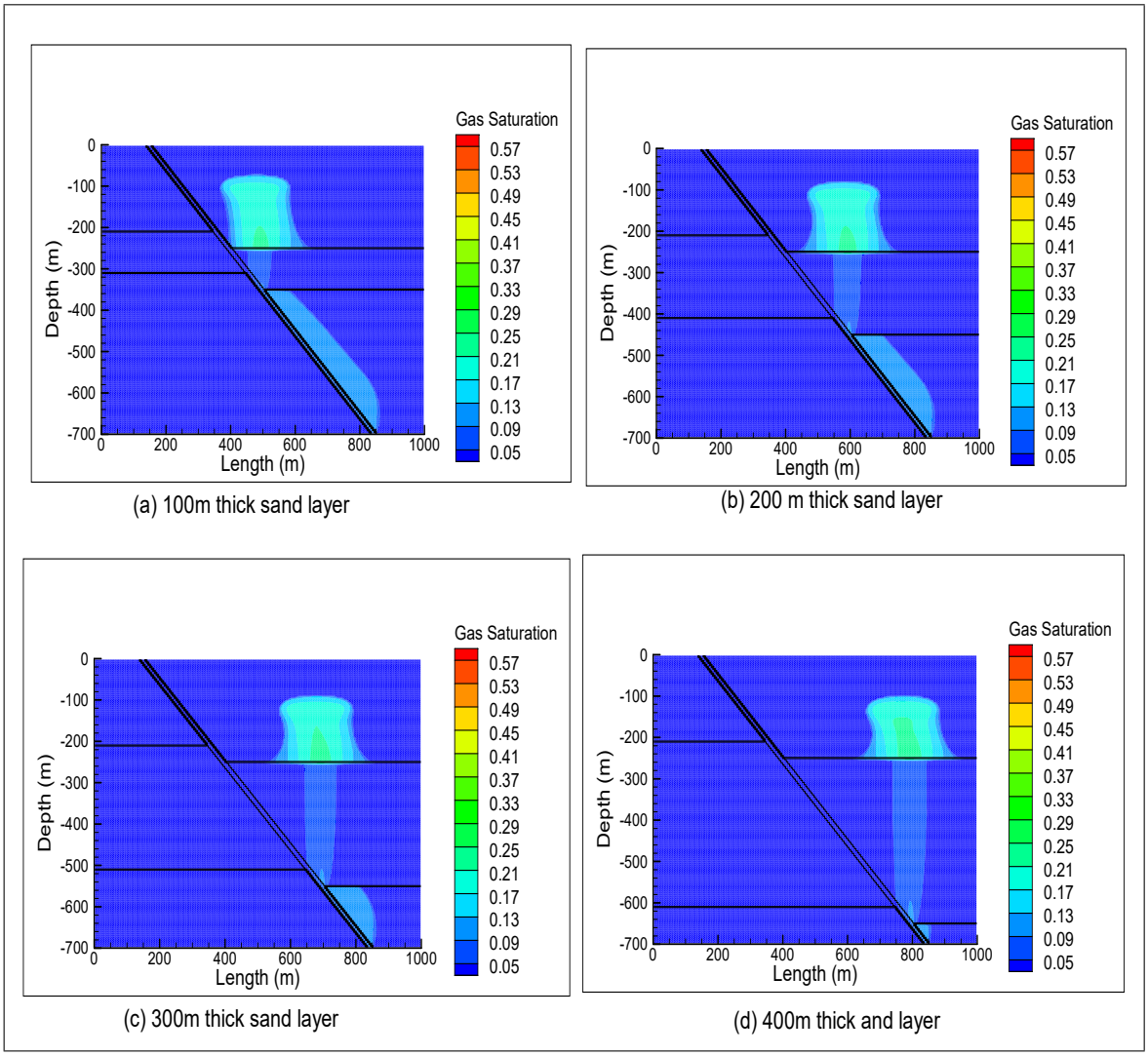

Figure 4.23: Gas saturation at the end of 100 years for different stratigraphic conditions

Similar to the gas saturation, the hydrate accumulation directly above the intersection point of fault zone and the sand layer indicates the importance of the sand zone in the gas migration into hydrate stability zone. The hydrate formation size and saturation is similar in all cases with the only noticeable difference in the location and difference in the shape (Figure 4.24). The average saturation remains at around 30-50% and highest about 60% in all cases. The hydrate accumulation region is observed to be shifted towards the hanging wall by more than 300m laterally comparing the 100m and 400m thick sand zones. Since the shift of 300m in hydrate accumulation region is a significant factor that may determine the well placement for methane gas production from hydrate reserves, it can be

concluded that stratigraphic changes are a significant factor to be considered in reservoir characterization and production planning.

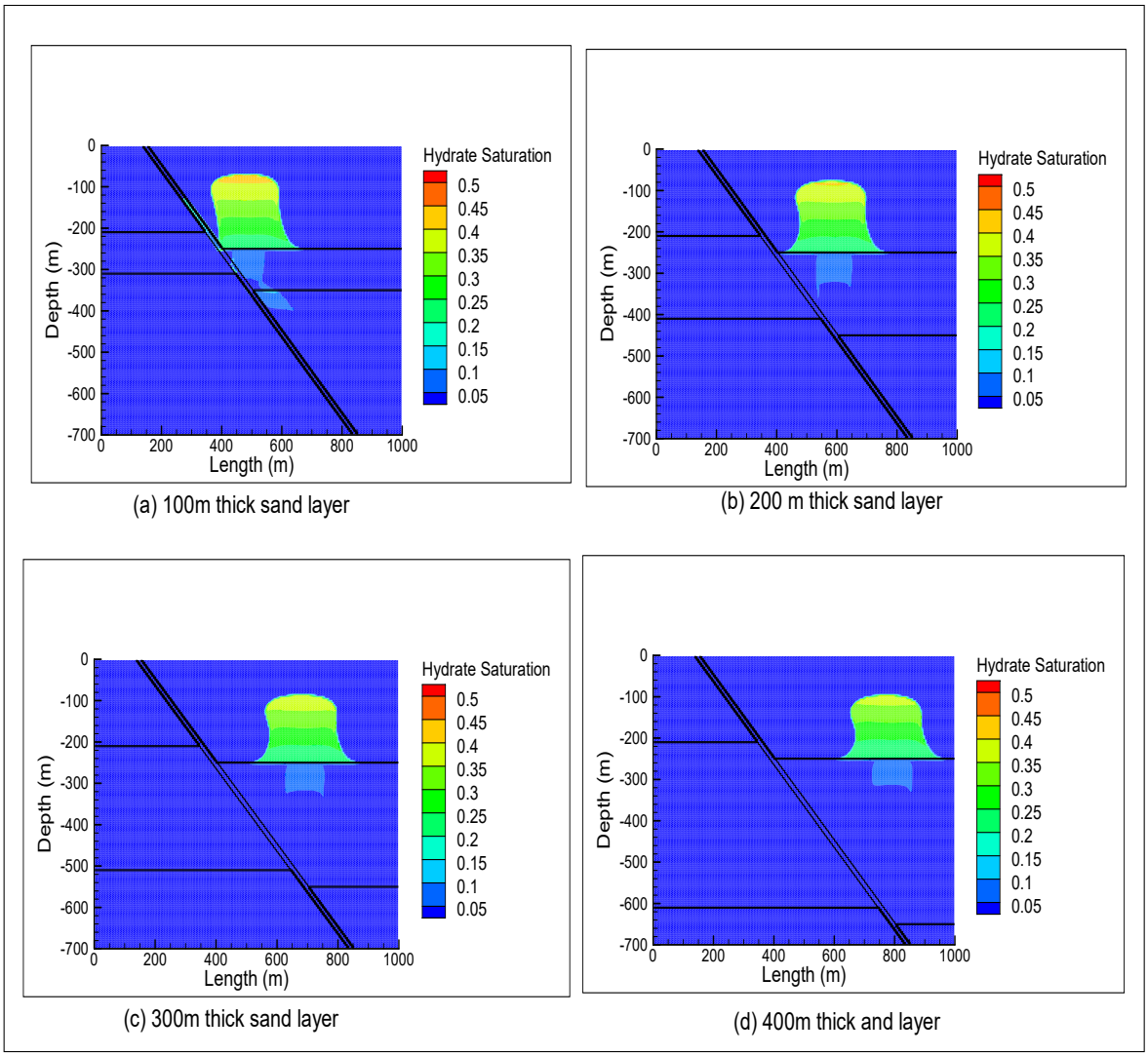

Figure 4.24: Hydrate saturation at the end of 100 years for different stratigraphic conditions

4.2.7 Grid Sensitivity

In order to validate the result obtained from the basecase model, grid sensitivity study was performed by simulating the basecase model with a 10m X 10m grid cell size. The result from the simulation shows that the total hydrates formed in the reservoir is at 7.78% within the result from the basecase model. The hydrate growth in the reservoir follows the

same trend as in the basecase model (Figure 4.25). Hydrate saturation distribution in the reservoir of the basecase model and the less refined model used in this senstivity model are comparable (Figure 4.26). It can be therefore infered that grid size has very little impact on the results obtained in this study.

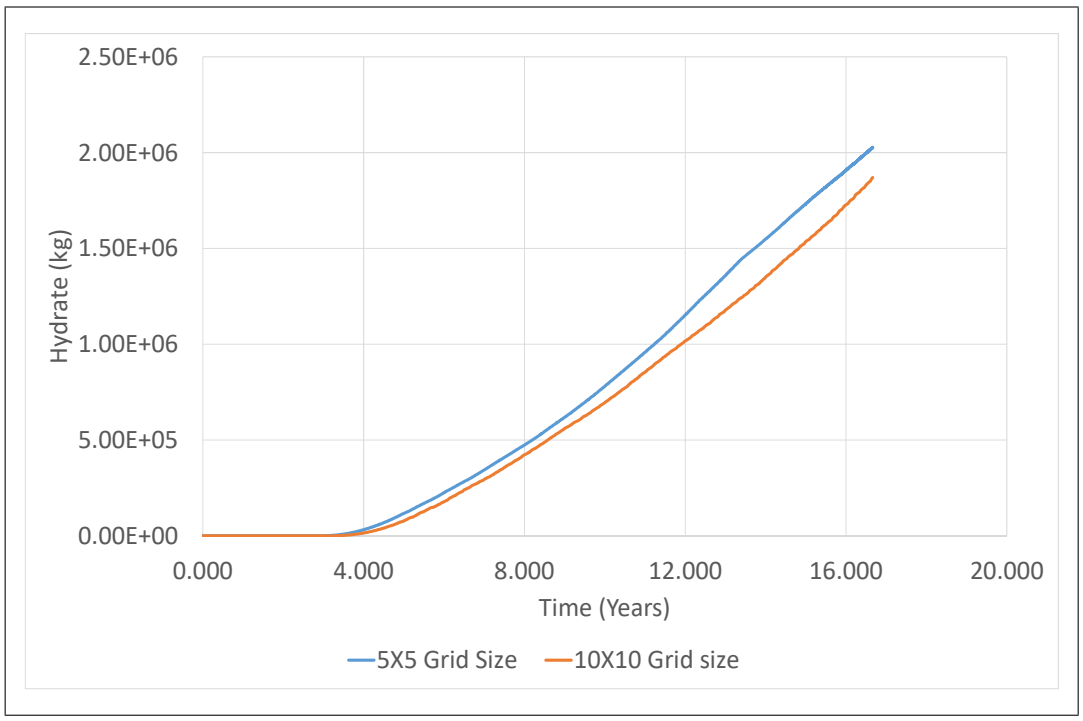

Figure 4.25: Hydrate growth in the reservoir for different grid sizes

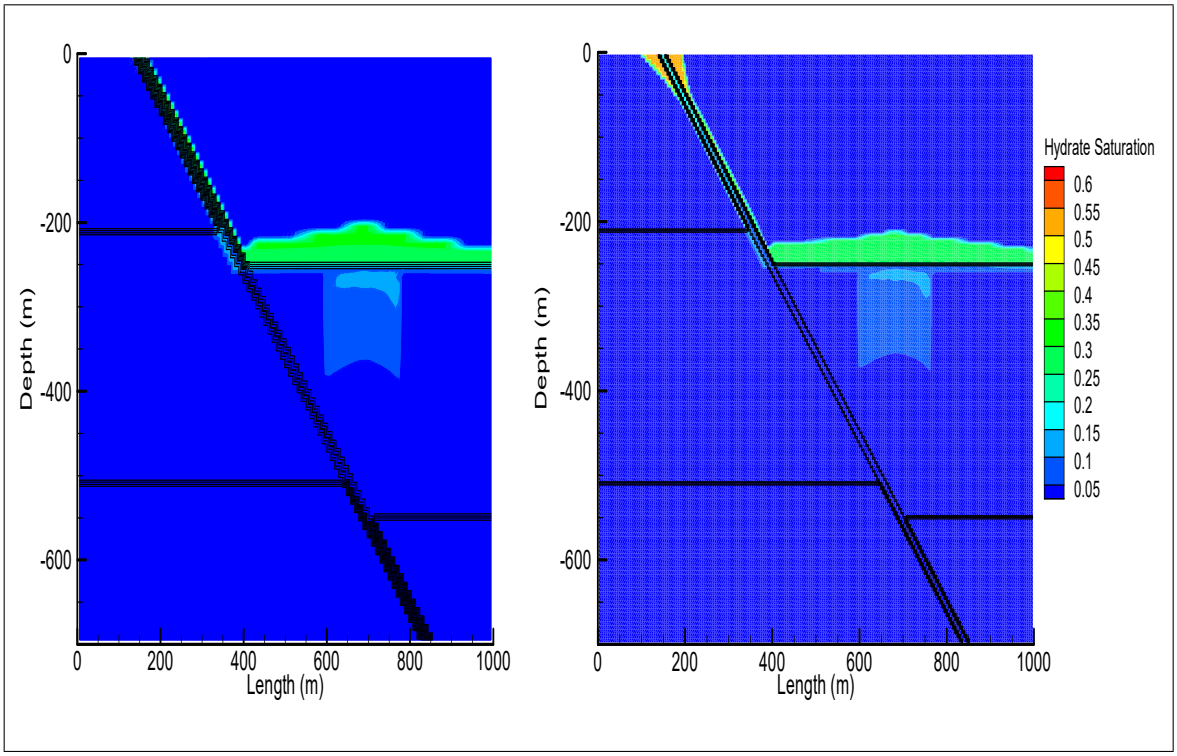

Figure 4.26: Hydrate saturation in the reservoir after 17 years for 10m x 10m grid size (left) and 5m x 5m grid size (right)

4.2.8 Summary of Findings

From the sensitivity results, it can be inferred that hydrate saturation is highly dependent on the flowrate and the salinity of the pore water in the reservoir. While flowrates of methane gas through the fault is an area of research that still does not have enough data, pore water salinity of reservoirs have been studied and can be obtained from well logs and core samples. These parameters must be taken into consideration in the reservoir characterization of gas hydrate reserves. The vertical location of gas hydrate accumulation was mostly impacted by the fault angle and the horizontal location by the stratigraphy. However, for different rock parameters these two properties change both lateral and vertical distribution of gas hydrates. The distribution of hydrate accumulation is also impacted by the permeability of the rocks, however, over long periods of gas flow, the effect is minimized. Boundary conditions also affect the spatial pattern as well as the saturation of gas

hydrates. A continuous boundary or a large reservoir facilitates the hydrate accumulation over a larger extent with lower saturation while a confined reservoir has highly saturated but lesser spatial extent of hydrates. All of these parameters have significant impact on the quality of gas hydrates reservoir and must be taken into account for reservoir characterization and production planning.

4.3 Lessons Learned for Future Modeling

The average resources required for a large reservoir model, albeit 2D, was significantly higher than expected. Due to the computational constraint, the models were run for a maximum of 72 hours and depending on the rock and fluid flow parameters, the simulation period greatly varied. There were other challenges in this study such as:

1. Difficulty in creating the geological model for an angled fault running through horizontal layers of rocks.
2. Limited number of time-steps that each simulation can be executed.
3. Very high computational time running on a single core machine.
4. Difficulty in solving the discretized equations resulting in a lack of convergence for certain flow conditions.
5. Computational errors that can arise due to the fact that the problem contains phase change and variable switching during the phase change.
6. Limited amount of literature and technical support available for the code due to it being mostly used for research purposes only.
7. Lack of definite data on the gas migration rate through fault in the Gulf of Mexico.

Some of these challenges were overcome during the course of the preliminary modeling. The creation of geological model was automated by writing a MATLAB code for this

problem which could be easily modified for further model creation. The maximum number of time steps were increased by changing the source code of TOUGH+HYDRATE. The computational time could not be significantly reduced but it was slightly reduced by using the High Performance Computers (HPC) at LSU and by executing multiple models at the same time in different nodes and cores. Convergence errors were eliminated by removing complexities in the simulations and by implementing overshoot values.

Despite the above, it is clear that the spatial and temporal distribution of thermogenic gas hydrates is not a mere function of attaining gas hydrate stability, but also dependent on existing structural and stratigraphic geometry, gas source volume and flow rates, fault activation times/period, pore water salinity, and sand/shale or geologic sequences in the area. This is particularly impactful if developing these resources - questions on whether to move updip of fault, or laterally adjacent to zones, whether to drill in sands and shales, or only sands, whether to expect a lateral continued hydrate body geometry, or a Christmas tree pattern need to be addressed and answered, and these reservoirs thoroughly characterized prior to development and production. Seismic and well log data are measured data on resource availability, but they are subject to interpretation, and not all sub-seismic characteristics can be obtained. Numerical simulations like those developed in this research can validate some of the geophysical data (and vice versa), and characterize at a scale not captured on seismic on inter-well correlations/interpretation.

Chapter 5
Conclusions

This research shows that numerical simulations can be used as an effective way of characterizing methane hydrate reserves. Existing numerical simulation tools for methane hydrate bearing sediments are focused towards production of methane gas from these hydrates. Due to the computational cost and complexities in modeling of formation of methane hydrates in the subsurface, this study demonstrates the limitations of these tools as well as the lack of data and research in this particular area of hydrate reservoir characterization.

Modeling of hydrate formation on the basecase model shows that hydrate formation primarily depends on the pressure and temperature conditions of the rock and the availability of methane gas. When the gas flow rate is high enough, the hydrate formation is significant even within a short period of time. Computational constraints play a major role in deducing the inferences that can be made from the base case model, especially pertaining to time required to form the hydrates. However, the hydrate geobody formation, saturation and the locations were in alignment with field studies and observations. As expected, the permeability of the hydrated zone decreased when hydrates accumulated in them due to the presence of solid hydrates in porous medium.

Sensitivity results show that the spatial and temporal distribution of the hydrate formation is however, not solely dependent on the pressure and temperature of the reservoir rock. Flow rate of methane gas up through the fault was one of the major parameters that affected the size and rate of hydrate formation with lower rate of flow not being enough for hydrate formation. The fault angle of hydrate formation also determines the rate of gas flow through the fault and hence the rate of formation of hydrates. The steeper the fault, the higher was the hydrate accumulation as the flow due to buoyancy was facilitated. Angle of fault zones determined the geobody formation and location of hydrate accumulations

with respect to the fault. Stratigraphic changes also impacted the formation of hydrates significantly as the thickness of the sand layer increased. Stratigraphic variation showed the shift in hydrate accumulation region by hundreds of meters which can be a significant factor in well placement. Varying the permeability also had a significant impact on the gas flow and hydrate formation region with higher permeability of sand zone facilitating higher flow into the gas hydrate stability zone. Pore water salinity of the reservoir changed the hydrate equilibrium condition and must be taken into account to determine the hydrate formation and saturation. Boundary conditions of the reservoir determined the distribution and saturation of the hydrates with highly saturated localized hydrates observed in confined reservoir and low saturation evenly distributed hydrates found in large or continuous reservoirs.

It was also evident that the current hydrate production and formation simulation codes are not equipped to simulate a full reservoir scale simulation of the formation process with many complexities that have to be simplified in order to not get computationally constrained. Future research in this area can be the coupling of geomechanical and geochemical aspects into the formation model as well as development of a robust, perhaps parallelized computational code that can simulate detailed complexities in the hydrate reservoirs.

Despite the current challenges, it can be definitively concluded that numerical simulations of gas hydrate formations constitute an important tool for hydrate reservoir character characterization, and must be employed prior to developing and producing from these reservoirs to determine long term reservoir management and production optimization strategies.

References

[1] J Bear. Dynamics of fluids in porous media. 1972.

[2] IM Boothroyd, S Almond, F Worrall, and RJ Davies. Assessing the fugitive emission of ch4 via migration along fault zones–comparing potential shale gas basins to non-shale basins in the uk. *Science of the total environment*, 580:412–424, 2017.

[3] Ray Boswell and Timothy S Collett. Current perspectives on gas hydrate resources. *Energy and environmental science*, 4(4):1206–1215, 2011.

[4] Ray Boswell, Timothy S Collett, Matthew Frye, William Shedd, Daniel R McConnell, and Dianna Shelander. Subsurface gas hydrates in the northern gulf of mexico. *Marine and Petroleum Geology*, 34(1):4–30, 2012.

[5] Ray Boswell, Dianna Shelander, Myung Lee, Tom Latham, Tim Collett, Gilles Guerin, George Moridis, Matthew Reagan, and Dave Goldberg. Occurrence of gas hydrate in oligocene frio sand: Alaminos canyon block 818: Northern gulf of mexico. *Marine and Petroleum Geology*, 26(8):1499–1512, 2009.

[6] James M Brooks, H Benjamin Cox, William R Bryant, MC Kennicutt, Robert G Mann, and Thomas J McDonald. Association of gas hydrates and oil seepage in the gulf of mexico. *Organic Geochemistry*, 10(1-3):221–234, 1986.

[7] JM Brooks, MC Kennicutt, RR Fay, TJ McDonald, and Roger Sassen. Thermogenic gas hydrates in the gulf of mexico. *Science*, 225(4660):409–411, 1984.

[8] Yuncheng Cao, Duofu Chen, and Lawrence M Cathles. A kinetic model for the methane hydrate precipitated from venting gas at cold seep sites at hydrate ridge, cascadia margin, oregon. *Journal of Geophysical Research: Solid Earth*, 118(9):4669–4681, 2013.

[9] Matthew Clarke and P Raj Bishnoi. Determination of the activation energy and intrinsic rate constant of methane gas hydrate decomposition. *The Canadian Journal of Chemical Engineering*, 79(1):143–147, 2001.

[10] Timothy S Collett, Arthur H Johnson, Camelia C Knapp, and Ray Boswell. Natural gas hydrates: a review. 2009.

[11] Timothy S. Collett, Myung W. Lee, Margarita V. Zyrianova, Stefan A. Mrozewski, Gilles Guerin, Ann E. Cook, and Dave S. Goldberg. Gulf of mexico gas hydrate joint industry project leg ii logging-while-drilling data acquisition and analysis. *Marine and Petroleum Geology*, 34(1):41 – 61, 2012. Resource and hazard implications of gas hydrates in the Northern Gulf of Mexico: Results of the 2009 Joint Industry Project Leg II Drilling Expedition.

[12] A. Cook, G. Guerin, S. Mrozewki, T.S. Collett, and R. Boswell. Gulf of mexico gas hydrate joint industry project leg ii: Walker ridge 313 lwd operations and results.

Proceedings of the Drilling and Scientific Results of the 2009 Gulf of Mexico Gas Hydrate Joint Industry Project Leg II, 2009.

[13] Arthur T Corey et al. The interrelation between gas and oil relative permeabilities. *Producers monthly*, 19(1):38–41, 1954.

[14] Jianchun Dai, Fred Snyder, Diana Gillespie, Adam Koesoemadinata, and Nader Dutta. Exploration for gas hydrates in the deepwater, northern gulf of mexico: Part i. a seismic approach based on geologic model, inversion, and rock physics principles. *Marine and Petroleum Geology*, 25(9):830 – 844, 2008. Thematic Set on Scientific Results of 2005 US DOE-Chevron JIP Drilling for Methane Hydrates Objectives in the Gulf of Mexico.

[15] Gerald R Dickens. Rethinking the global carbon cycle with a large, dynamic and microbially mediated gas hydrate capacitor. *Earth and Planetary Science Letters*, 213(3):169–183, 2003.

[16] Gerald R Dickens. Down the rabbit hole: Toward appropriate discussion of methane release from gas hydrate systems during the paleocene-eocene thermal maximum and other past hyperthermal events. *Climate of the Past*, 7(3):831–846, 2011.

[17] Gerald R Dickens and Mary S Quinby-Hunt. Methane hydrate stability in seawater. *Geophysical Research Letters*, 21(19):2115–2118, 1994.

[18] P. Englezos, N. Kalogerakis, P. D. Dholabhai, and P. R. Bishnoi. Kinetics of formation of methane and ethane gas hydrates. *Chemical Engineering Science*, 42(11):2647–2658, 1987.

[19] J Forrest, E Marcucci, and P Scott. Geothermal gradients and subsurface temperatures in northern gulf of mexico: Search and discovery article no. 30048, 2007.

[20] Matthew Frye, William Shedd, and Ray Boswell. Gas hydrate resource potential in the terrebonne basin, northern gulf of mexico. *Marine and Petroleum geology*, 34(1):150–168, 2012.

[21] GD Ginsburg and VA Soloviev. Mud volcano gas hydrates in the caspian sea. *Bulletin of the Geological Society of Denmark*, 41(95):100, 1994.

[22] Gilles Guerin, Ann Cook, Stefan Mrozewski, Timothy Collett, and Ray Boswell. Gulf of mexico gas hydrate joint industry project leg ii. *Green Canyon 955 LWD operations and results*, 2010.

[23] Seth S. Haines, Patrick E. Hart, Timothy S. Collett, William Shedd, Matthew Frye, Paul Weimer, and Ray Boswell. High-resolution seismic characterization of the gas and gas hydrate system at green canyon 955, gulf of mexico, usa. *Marine and Petroleum Geology*, 82:220 – 237, 2017.

[24] EG Hammerschmidt. Formation of gas hydrates in natural gas transmission lines. *Industrial and Engineering Chemistry*, 26(8):851–855, 1934.

[25] Martin Hovland and Ove Tobias Gudmestad. Potential influence of gas hydrates on seabed installations. *Natural gas hydrates: occurrence, distribution, and detection*, pages 307–315, 2001.

[26] VT John, KD Papadopoulos, and GD Holder. A generalized model for predicting equilibrium conditions for gas hydrates. *AIChE Journal*, 31(2):252–259, 1985.

[27] Gil Young Kim, Bo Yeon Yi, Dong Geun Yoo, Byong Jae Ryu, and Michael Riedel. Evidence of gas hydrate from downhole logging data in the ulleung basin, east sea. *Marine and Petroleum Geology*, 28(10):1979–1985, 2011.

[28] HC Kim, PR Bishnoi, RA Heidemann, and SSH Rizvi. Kinetics of methane hydrate decomposition. *Chemical engineering science*, 42(7):1645–1653, 1987.

[29] Masanori Kurihara, Kunihiro Funatsu, Hisanao Ouchi, Yoshihiro Masuda, Koji Yamamoto, Hideo Narita, Scott R Dallimore, Timothy S Collett, and Steve H Hancock. Analyses of production tests and mdt tests conducted in mallik and alaska methane hydrate reservoirs: what can we learn from these well tests. In *Proceedings from the 6th International Conference of Gas Hydrates*, 2008.

[30] KA Kvenvolden. A primer on the geological occurrence of gas hydrate. *Geological Society, London, Special Publications*, 137(1):9–30, 1998.

[31] Keith A Kvenvolden and Mark A McMenamin. Hydrates of natural gas: a review of their geologic occurrence. 1980.

[32] Laura L Lapham, Marc Alperin, Jeffrey Chanton, and Chris Martens. Upward advection rates and methane fluxes, oxidation, and sources at two gulf of mexico brine seeps. *Marine Chemistry*, 112(1-2):65–71, 2008.

[33] IR MacDonald, NL Guinasso Jr, R Sassen, JM Brooks, L Lee, and KT Scott. Gas hydrate that breaches the sea floor on the continental slope of the gulf of mexico. *Geology*, 22(8):699–702, 1994.

[34] Yuri F Makogon. A gas hydrate formation in the gas saturated layers under low temperature. *Gas Industry*, 5:14–15, 1965.

[35] Yuri F Makogon. Natural gas hydratesa promising source of energy. *Journal of Natural Gas Science and Engineering*, 2(1):49–59, 2010.

[36] G Edward Manger et al. Porosity and bulk density of sedimentary rocks. 1963.

[37] Alexei V Milkov and Roger Sassen. Thickness of the gas hydrate stability zone, gulf of mexico continental slope. *Marine and petroleum Geology*, 17(9):981–991, 2000.

[38] George J Moridis. Tough+ hydrate v1. 2 user's manual: A code for the simulation of system behavior in hydrate-bearing geologic media. 2014.

[39] GJ Moridis. Numerical studies of gas production from methane hydrates. In *SPE Gas Technology Symposium*. Society of Petroleum Engineers, 2002.

[40] Heng-Joo Ng and Donald B Robinson. The measurement and prediction of hydrate formation in liquid hydrocarbon-water systems. *Industrial and Engineering Chemistry Fundamentals*, 15(4):293–298, 1976.

[41] William R Parrish and John M Prausnitz. Dissociation pressures of gas hydrates formed by gas mixtures. *Industrial and Engineering Chemistry Process Design and Development*, 11(1):26–35, 1972.

[42] Ingo A Pecher. Oceanography: Gas hydrates on the brink. *Nature*, 420(6916):622, 2002.

[43] John W Pohlman, Elizabeth A Canuel, N Ross Chapman, George D Spence, Michael J Whiticar, and Richard B Coffin. The origin of thermogenic gas hydrates on the northern cascadia margin as inferred from isotopic (13 c/12 c and d/h) and molecular composition of hydrate and vent gas. *Organic Geochemistry*, 36(5):703–716, 2005.

[44] AW Rempel and BA Buffett. Mathematical models of gas hydrate accumulation. *Geological Society, London, Special Publications*, 137(1):63–74, 1998.

[45] C Ruppel, R Boswell, and E Jones. Scientific results from gulf of mexico gas hydrates joint industry project leg 1 drilling: introduction and overview. *Marine and Petroleum Geology*, 25(9):819–829, 2008.

[46] Carolyn Ruppel. Tapping methane hydrates for unconventional natural gas. *Elements*, 3(3):193–199, 2007.

[47] Jonny Rutqvist and Chin-Fu Tsang. Tough-flac: a numerical simulator for analysis of coupled thermal-hydrologic-mechanical processes in fractured and porous geological media under multi-phase flow conditions. In *Proceedings of the TOUGH Symposium*, pages 12–14, 2003.

[48] Roger Sassen and Ian R Macdonald. Hydrocarbons of experimental and natural gas hydrates, gulf of mexico continental slope. *Organic Geochemistry*, 26(3-4):289–293, 1997.

[49] M. S. Selim and E. D. Sloan. Heat and mass transfer during the dissociation of hydrates in porous media. *AIChE journal*, 35(6):1049–1052, 1989.

[50] N Shakhova, I Semiletov, I Leifer, A Salyuk, P Rekant, and D Kosmach. Geochemical and geophysical evidence of methane release over the east siberian arctic shelf. *Journal of Geophysical Research: Oceans*, 115(C8), 2010.

[51] E. D. Sloan. Physical/chemical properties of gas hydrates and application to world margin stability and climatic change. *Geological Society, London, Special Publications*, 137(1):31–50, 1998.

[52] E. D. Sloan. Fundamental principles and applications of natural gas hydrates. *Nature*, 426(6964):353–363, 2003.

[53] E. D. Sloan and Carolyn Koh. *Clathrate hydrates of natural gases*. CRC press, 2007.

[54] Fred FC Snyder, Lecia K Muller, Nader Dutta, Deborah R Hutchinson, Patrick E Hart, Myung W Lee, Brandon Dugan, Carolyn Ruppel, WT Wood, Richard Coffin, et al. Seismic analysis and characterization of gas hydrates in the northern deepwater gulf of mexico. *AAPG Bull*, 88:13, 2004.

[55] Hideaki Takahashi, Tetsuo Yonezawa, Ed Fercho, et al. Operation overview of the 2002 mallik gas hydrate production research well program at the mackenzie delta in the canadian arctic. In *Offshore Technology Conference*. Offshore Technology Conference, 2003.

[56] JH Van der Waals and JC Platteeuw. Clathrate solutions. *Advances in Chemical Physics, Volume 2*, pages 1–57, 1959.

[57] M Th Van Genuchten. A closed-form equation for predicting the hydraulic conductivity of unsaturated soils 1. *Soil science society of America journal*, 44(5):892–898, 1980.

[58] Matthew R Walsh, Steve H Hancock, Scott J Wilson, Shirish L Patil, George J Moridis, Ray Boswell, Timothy S Collett, Carolyn A Koh, and E Dendy Sloan. Preliminary report on the commercial viability of gas production from natural gas hydrates. *Energy Economics*, 31(5):815–823, 2009.

[59] Thomas Walsh, Peter Stokes, Manmath Panda, Tom Morahan, David Greet, Steve MacRae, North Slope Borough, Praveen Singh, Shirish Patil, and AK Fairbanks. Characterization and quantification of the methane hydrate resource potential associated with the barrow gas fields. In *Proceedings of the 6th International Conference on Gas Hydrotes (ICGH), Vancouver, British Columbia, Canada*. Citeseer, 2008.

[60] G Westbrook, B Carson, and R Musgrave. Shipboard scientific party, 1994. *Initial reports of the Ocean Drilling Program*, 146(pt 1), 1994.

[61] WT Wood, JF Gettrust, NR Chapman, GD Spence, and RD Hyndman. Decreased stability of methane hydrates in marine sediments owing to phase-boundary roughness. *Nature*, 420(6916):656, 2002.

[62] Wenyue Xu and Carolyn Ruppel. Predicting the occurrence, distribution, and evolution of methane gas hydrate in porous marine sediments. *Journal of Geophysical Research: Solid Earth*, 104(B3):5081–5095, 1999.

[63] Koji Yamamoto. Overview and introduction: Pressure core-sampling and analyses in the 20122013 mh21 offshore test of gas production from methane hydrates in the eastern nankai trough. *Marine and Petroleum Geology*, 66:296 – 309, 2015. Gas hydrate drilling in Eastern Nankai.

[64] Lili Zheng, Hui Zhang, Mingyu Zhang, Prasad Kerkar, and Devinder Mahajan. Modeling methane-hydrate formation in marine sediments. 2009.

Appendix A
MATLAB Code for Model Creation

```
%% No Inhibitor 1-Intial Phase Model Creation
close all
clear all
%% Defining Geometry
prompt2 = 'Enter the height of the reservoir(m)\n';
z = input (prompt2);
prompt3 = 'Enter the height of the first shale layer (m)\n';
height_shale = input(prompt3);
prompt4 = 'Enter the height of the sand layer(m) \n';
height_sand = input(prompt4);
prompt5 ='Enter the horizontal width of the fault(m) \n';
width_fault = input(prompt5);
prompt7 ='Enter the slippage height(m) \n';
fault_slippage = input(prompt7);
prompt8 = 'Enter fault angle (degree)';
FA  = input(prompt8);
height_shale2 = z-height_shale-height_sand;
y = 1;
x_size = 10;
y_size = 1;
z_size = 10;
%topshale = 10E5;   %Only used for Boundary conditions
%sideshale = 10E5;  %Only used for Boundary conditions
fault_angle = FA;
theta = 90-fault_angle;
% x_temp = z/tand(FA) +1000;     %Only used for fault angles
% x=round(x_temp,-2);            %Only used for fault angles
x = 1000;
shala_x1 = ((x/2)-(width_fault)-(tand(theta)*z/2));
shala_x2 = shala_x1+(tand(theta)*(height_shale-fault_slippage));
shala_z1 = 0;
shala_z2 = height_shale-fault_slippage;
sanda_x1 = shala_x2;
sanda_x2 = sanda_x1+tand(theta)*(height_sand);
shalb_x1 = sanda_x2;
shalb_x2 = shalb_x1+tand(theta)*(height_shale2+fault_slippage);
shalb_z1 = shala_z2+height_sand;
shalc_x1 = shala_x1+width_fault;
shalc_x2 = shalc_x1+(tand(theta)*(height_shale));
sandb_x1 = shalc_x2;
```

```
sandb_x2 = sandb_x1+tand(theta)*(height_sand);
shald_x1 = sandb_x2;
shald_x2 = shald_x1+tand(theta)*(height_shale2);
%defining boundaries for each rocktypes
shala_x = [
    0
    shala_x1
    shala_x2
    0
    0];
shala_z = [
    0
    0
    shala_z2
    shala_z2
    0];
shalb_x = [
    0
    shalb_x1
    shalb_x2
    0
    0];
shalb_z = [
    shalb_z1
    shalb_z1
    z
    z
    shalb_z1];
shalc_x = [
    shalc_x1
    x
    x
    shalc_x2
    shalc_x1];
shalc_z = [
    0
    0
    height_shale
    height_shale
    0];
shald_x = [
    shald_x1
    x
    x
    shald_x2
```

```
    shald_x1];
shald_z = [
    height_shale+height_sand
    height_shale+height_sand
    z
    z
    height_shale+height_sand];
sanda_x = [
    0
    sanda_x1
    sanda_x2
    0
    0];
sanda_z = [
    shala_z2
    shala_z2
    shala_z2+height_sand
    shala_z2+height_sand
    shala_z2];
sandb_x = [
    sandb_x1
    x
    x
    sandb_x2
    sandb_x1];
sandb_z = [
    height_shale
    height_shale
    height_shale+height_sand
    height_shale+height_sand
    height_shale];
fault_x = [
    shala_x1
    shala_x1+width_fault
    shalb_x2+width_fault
    shalb_x2
    shala_x1];
fault_z = [
    0
    0
    z
    z
    0];
% topshale_x = [
%     0
```

```
%     x
%     x
%     0
%     0];
% topshale_z = [
%     0
%     0
%     -topshale
%     -topshale
%     0];
% Used for boundary conditions
% sideshale_xl = [
%     -sideshale
%     0
%     0
%     -sideshale
%     -sideshale];
% sideshale_zl = [
%     z
%     z
%     -topshale
%     -topshale
%     z];
% sideshale_xr = [
%     x
%     x+sideshale
%     x+sideshale
%     x
%     x];
% sideshale_zr = [
%     z
%     z
%     -topshale
%     -topshale
%     z];

%% Rocktype
rocks = {'Shale' 'Shala' 'Shalb' 'Shalc' 'Shald' 'Sanda' 'Sandb' 'Fault'};
%% Defining grids
clc
x_mesh1 = ((x_size/2):x_size:x);
z_mesh1 = ((z_size/2):z_size:z);
x_mesh = x_mesh1;
z_mesh = z_mesh1;
y_mesh = y/2;
```

```
xl=length(x_mesh(1,:));
zl=length(z_mesh(1,:));
elem_vol = x_size*z_size*y_size;
% elem_vol2 = topshale*x_size*y_size;
[x_grid1, z_grid1]=meshgrid(x_mesh, z_mesh);
x_grid = x_grid1(:);
nn = size(x_grid,1);
z_grid = z_grid1(:);
y_grid = (repelem(y_mesh,nn))';
elem_volume= (repelem(elem_vol,nn))';
elem_aht=zeros(nn,1);
for c4 = 1:nn
    if mod(c4,zl)==0 || mod(c4,zl)==1
        elem_aht(c4,1)= x_size*y_size;
    end
end
data_co = [elem_volume elem_aht x_grid y_grid z_grid];
data_co2 = num2cell(data_co);
nnx=round((nn/8));
id=num2cell(find(x_grid));
data_main = [id id data_co2];
[ina,ona]= inpolygon(x_grid,z_grid,shala_x,shala_z);
inona=ina | ona;
ida =num2cell(find(inona(:)));
for c1 = 1:nn
    for c2 = 1:size(ida,1)
        if isequal(ida{c2,1}, id{c1,1})
            data_main{c1,2}='Shala';
        end
    end
end
[inb,onb]= inpolygon(x_grid,z_grid,shalb_x,shalb_z);
inonb=inb | onb;
idb =num2cell(find(inonb(:)));
for c1 = 1:nn
    for c2 = 1:size(idb,1)
        if isequal(idb{c2,1}, id{c1,1})
            data_main{c1,2}='Shalb';
        end
    end
end
[inc,onc]= inpolygon(x_grid,z_grid,shalc_x,shalc_z);
inonc=inc | onc;
idc =num2cell(find(inonc(:)));
for c1 = 1:nn
```

```
    for c2 = 1:size(idc,1)
        if isequal(idc{c2,1}, id{c1,1})
            data_main{c1,2}='Shalc';
        end
    end
end
[ind,ond]= inpolygon(x_grid,z_grid,shald_x,shald_z);
inond=ind | ond;
idd =num2cell(find(inond(:)));
for c1 = 1:nn
    for c2 = 1:size(idd,1)
        if isequal(idd{c2,1}, id{c1,1})
            data_main{c1,2}='Shald';
        end
    end
end
[insa,onsa]= inpolygon(x_grid,z_grid,sanda_x,sanda_z);
inonsa=insa | onsa;
idsa =num2cell(find(inonsa(:)));
for c1 = 1:nn
    for c2 = 1:size(idsa,1)
        if isequal(idsa{c2,1}, id{c1,1})
            data_main{c1,2}='Sanda';
        end
    end
end
[insb,onsb]= inpolygon(x_grid,z_grid,sandb_x,sandb_z);
inonsb=insb | onsb;
idsb =num2cell(find(inonsb(:)));
for c1 = 1:nn
    for c2 = 1:size(idsb,1)
        if isequal(idsb{c2,1}, id{c1,1})
            data_main{c1,2}='Sandb';
        end
    end
end
[inf,onf]= inpolygon(x_grid,z_grid,fault_x,fault_z);
inonf=inf | onf;
idf =num2cell(find(inonf(:)));
for c1 = 1:nn
    for c2 = 1:size(idf,1)
        if isequal(idf{c2,1}, id{c1,1})
            data_main{c1,2}='Fault';
        end
    end
```

```
end
% Used for boundary conditions
% [int,ont]= inpolygon(x_grid,z_grid,topshale_x,topshale_z);
% inont=int | ont;
% idt =num2cell(find(inont(:)));
% for c1 = 1:nn
%     for c2 = 1:size(idt,1)
%         if isequal(idt{c2,1}, id{c1,1})
%             data_main{c1,2}='Shale';
%             data_main{c1,3}=topshale*x_size*y_size;
%     end
%     end
% end
% [insl,onsl]= inpolygon(x_grid,z_grid,sideshale_xl,sideshale_zl);
% inonsl=insl | onsl;
% idsl =num2cell(find(inonsl(:)));
% for c1 = 1:nn
%     for c2 = 1:size(idsl,1)
%         if isequal(idsl{c2,1}, id{c1,1})
%             data_main{c1,2}='Shale';
%             data_main{c1,3}=z_size*sideshale*y_size;
%     end
%     end
% end
% [insr,onsr]= inpolygon(x_grid,z_grid,sideshale_xr,sideshale_zr);
% inonsr=insr | onsr;
% idf =num2cell(find(inonsr(:)));
% for c1 = 1:nn
%     for c2 = 1:size(idf,1)
%         if isequal(idf{c2,1}, id{c1,1})
%             data_main{c1,2}='Shale';
%             data_main{c1,3}=z_size*sideshale*y_size;
%     end
%     end
% end

for c1 = 1:nn
    data_main{c1,7} = (data_main{c1,7}*(-1));
end
%visualization of the created model
figure;
plot(shala_x,-1*shala_z,'y');
hold on;
plot(shalb_x,-1*shalb_z,'y');
plot(shalc_x,-1*shalc_z,'y');
```

```
plot(shald_x,-1*shald_z,'y');
plot(sanda_x,-1*sanda_z,'b');
plot(sandb_x,-1*sandb_z,'b');
plot(fault_x,-1*fault_z,'r');
hold off;
figure;
fill(shala_x,-1*shala_z,'y');
hold on;
fill(shalb_x,-1*shalb_z,'y');
fill(shalc_x,-1*shalc_z,'y');
fill(shald_x,-1*shald_z,'y');
fill(sanda_x,-1*sanda_z,'b');
fill(sandb_x,-1*sandb_z,'b');
fill(fault_x,-1*fault_z,'r');
% plot(topshale_x,topshale_z);
% plot(sideshale_xl,sideshale_zl);
% plot(sideshale_xr,sideshale_zr);
% plot(x_grid(ina),z_grid(ina),'r+');
% plot(x_grid(inb),z_grid(inb),'go');
% plot(x_grid(inc),z_grid(inc),'r+');
% plot(x_grid(ind),z_grid(ind),'go');
% plot(x_grid(insa),z_grid(insa),'b+');
% plot(x_grid(insb),z_grid(insb),'b+');
% plot(x_grid(inf),z_grid(inf),'yo');

hold off;
%% Defining Connections
numcon = zl*(xl-1)+xl*(zl-1);
con1={};
con2={};
con3={};
con4={};
con={};
conx={};
data_conn={};
data_connection={};
for c6= 1:1:xl
    for c7=(c6*zl-(zl-1)):1:(c6*zl-1)
         con1{c7,1} = data_main{c7,1};
         con2{c7,1} = con1{c7,1}+1;
    end
end
con=[con1 con2];
for c8= 1:1:zl
    for c9=c8:zl:(zl*xl-(2*zl-c8))
```

```
            con3{c9,1} = data_main{c9,1};
            con4{c9,1} = con3{c9,1}+zl;
        end
    end
    conx=[con3 con4];
    data_conn=[
        con
        conx];
    ISE = cellfun('isempty',data_conn); % find empty cells
    Q = any(ISE,2); % true for rows with 1+ empty values
    data_conn(Q,:) = []; % remove those rows
    for c1 = 1: length(data_conn)
        if c1 <= (xl*(zl-1))
            conxki{c1,1} = 3;
            conxD{c1,1} = z_size/2;
            conxD{c1,2} = z_size/2;
            conxA{c1,1} = x_size*y_size;
            conxB{c1,1} = 1;
        else
            conxki{c1,1} =1;
            conxD{c1,1} = x_size/2;
            conxD{c1,2} = x_size/2;
            conxA{c1,1} = z_size*y_size;
            conxB{c1,1} = 0;

        end
    end
    data_connection=[data_conn conxki conxD conxA conxB];

    %% Writing Files
    Title_1='ELEME\n';
    Title_2='\nCONNE\n';
    Title_3='GENER\n';
    lastline='\n';
    GX=1.0E-3;
    EX=3.463e+05;
        fileID =fopen(['c:/HYDRATES/tests/MESH'],'w');
        fileIDM=fopen(['c:/HYDRATES/tests/GENER'],'w');
    if fileID<0
        printf('error opening file');
        return;
    end
    if fileIDM<0
        printf('error opening file');
```

```
    return;
end
fprintf(fileIDM,Title_3);
formatinj = '%5dInj%02d                                    %s %10.3e%10.3e\n';

for cn=1:nn
    lastrow = min(data_main{cn,7});
end
ss=0;
for cn=1:nn
    if strcmp(data_main{cn,2},'Fault')
        if data_main{cn,7}== lastrow
            ss=ss+1;
            fprintf(fileIDM,formatinj,data_main{cn,1},ss,'COM2',GX,EX);
        end
    end
end
fprintf(fileIDM,lastline);
fclose(fileIDM);
fprintf(fileID,Title_1);
formatspec='%5d          %s%10.3e%10.3e          %10.3e%10.3e%10.3e\n';

for c5 = 1:nn
    fprintf(fileID,formatspec,data_main{c5,:});
end
formatspec2='%5d%5d                %5d%10.3e%10.3e%10.3e%10.3e\n';
fprintf(fileID,Title_2);
for c5 = 1:numcon
    fprintf(fileID,formatspec2,data_connection{c5,:});
end
fprintf(fileID,lastline);
fclose(fileID);

%% INCON
% phi_0 = 0.65;          %Used if Porosity is defined by Athy's law
% phi_c = 0.51E-3;       %Used if Porosity is defined by Athy's law
% W_d = 2112.5;          %Used if Porosity is defined by Athy's law

sandphi = 0.35;
shalephi = 0.15;
faultphi = 0.50;
sandperm = [
    1.00E-12
    1.00E-12
    1.00E-13];
```

```
shaleperm = [
    1.00E-14
    1.00E-14
    1.00E-15];
faultperm = [
    1.00e-11
    1.00e-11
    1.00e-12];
topperm = [
    1.00e-14
    1.00e-14
    1.00E-15];
Sur_Pres = 2.08909E+07; %sea floor pressure
Sur_Temp = 1.0e+1; %sea floor temp
pres_grad = 10000;
temp_grad = 32e-3;
XmA = 2e-4;
S_hyd = 2e-5;
XiA = 1e-6;
% Writing INCON file
Title_4='INCON\n';
lastline='\n';



    fileID =fopen(['c:/HYDRATES/tests/INCON'],'w');
if fileID<0
    printf('error opening file');
    return;
end
fprintf(fileID,Title_4);
formatspeca='%5d            %10.8e  Aqu: P,            , X__ma, X_i_A, T
%10.8e %10.8e %10.8e\n';
formatspecb='     %10.9e      %10.9e      %10.9e      %10.9e\n';
for c10 = 1:nn
    if (strcmp(data_main{c10,2},'Sanda')==1||strcmp(data_main{c10,2},'Sandb')

        perm = sandperm';
        phi =sandphi;
    elseif (strcmp(data_main{c10,2},'Shala')==1||strcmp(data_main{c10,2},'Sha

        perm = shaleperm';
        phi = shalephi;
    elseif (strcmp(data_main{c10,2},'Fault')==1)
```

```
        perm = faultperm';
        phi= faultphi;
    else

        perm = topperm';
        phi = shalephi;
    end
    %phi = phi_0*exp(phi_c*(data_main{c10,7}-W_d)); (For Athy's Law, not used
    pressure = Sur_Pres-pres_grad*data_main{c10,7};
    temperature = Sur_Temp-temp_grad*data_main{c10,7};
    fprintf(fileID,formatspeca,data_main{c10,1},phi,perm);
    fprintf(fileID, formatspecb,pressure,XmA,XiA,temperature);


end

fprintf(fileID,lastline);
fclose(fileID);
```

Vita

Sulav Dhakal was born in 1992, in Kathmandu, Nepal. He graduated with a Bachelor in Civil Engineering from Tribhuvan University, Nepal in 2013. Upon graduation, he worked as a freelance engineer working in various projects for a year before joining DesignCore Systems, an engineering firm specializing in hydrological study and design, where he worked for 2 years. Thereafter, he moved to the United States of America to pursue graduate education. He is currently a candidate for MS in Petroleum Engineering, to be awarded in May 2018. Sulav is also looking to continue his study pursuing PhD in Petroleum Engineering.